LUNAR AND SOLAR MAGNETIC VARIATIONS AT ABINGER: THEIR DETECTION AND ESTIMATION BY SPECTRAL ANALYSIS VIA FOURIER TRANSFORMS

By D. I. BLACK

Imperial Chemical Industries Ltd, Organic House, Billingham, Teeside

CONTENTS

The geomagnetic field measured at any point on Earth as a function of time shows periodic variations due to atmospheric processes. A method of time series analysis based on discrete Fourier transforms is developed for the detection and estimation of lines in the frequency spectrum; the method gives estimates, with error limits, of the amplitudes of sinusoidal variations in the data, and these estimates are unbiased by noise. The method is used to determine the lunar and solar variations present in Abinger declination records, data for a period of 17 years (1927–56) being used. The coherence between Abinger

data and time series that model the lunar and solar input functions to the atmosphere aids the identification of lines in the Abinger spectrum. The amplitude spectrum of magnetic declination at Abinger shows prominent solar peaks at 1, 2, 3, 4 cycles per day (c/d), and lunar peaks at 0.0703, 1.932, and 2.932 c/d. Sidebands of the solar diurnal peak at 1 ± 0.037 c/d are attributed to a solar rotation mechanism, and this is supported by a high resolution power spectrum that shows the width of these sidebands. The high resolution analysis also shows annual and semi-annual splitting of the solar diurnal and semi-diurnal lines, and of the lunar semi-diurnal line.

1. INTRODUCTION

Many workers have extracted from magnetic records the amplitude and phase of periodic variations ascribed to solar and lunar influences on the atmosphere. Most previous workers (for example, Chapman 1913, 1957; Bartels & Johnston 1940; Cain 1957; Wilkes 1962; Schneider 1963; Leaton, Malin & Finch 1963) have used a method of analysis similar to that described by Chapman & Miller (1940) and Tschu (1949) and termed here the C.–M. method. The majority of workers have restricted their investigations of lunar variations to those arising from the semi-diurnal component of lunar gravity, but a few have attempted the identification of other lunar variations (see, for example, Schneider 1963; Leaton *et al.* 1963).

The first step of the C.–M. method is to sum data recorded at the same phase of the moon to obtain an average daily record for each part of a lunation. Two sets of Fourier transforms are then calculated; the first obtains the harmonics of each daily record, and the second analyses the variation over the lunation of each daily harmonic. Combinations of the Fourier coefficients of the second analysis give the different lunar variations.

The C.–M. method has many advantages. Principal among these are the method's ability to analyse broken data sequences (and hence one may select the days to be analysed by season, sunspot number, magnetic character figure, etc.), and the method's association of a probable error with the estimates of amplitude and phase of a magnetic variation. The disadvantages of the C.–M. method become apparent when it is compared with the techniques of power spectrum analysis (see Blackman & Tukey (1958) for an early exposition). The C.–M. method fails to give any bandwidth for its estimates: all methods of time series analysis can only give estimates of amplitude and phase that are an average over a band of frequencies. For the estimates to be meaningful, the bandwidth must be known, and it must be sufficiently small for there to be no overlap between 'lines' in the spectrum. However, the C.–M. method can only determine the parameters of magnetic variations of pre-specified frequencies, and it does not examine the spectrum; there is thus no check that the spectral line under investigation (i.e. the magnetic variation being sought, in the present application) is not contaminated by other nearby lines. The C.–M. method has the further weakness of being unable to search for so far undetected variations unless their frequency is predicted by theory.

Gupta (1966) and Gupta & Chapman (1969) have used power spectrum analysis to identify lunar variations. They follow the techniques described by Blackman & Tukey (1958), and obtain their power spectra from the autocorrelation function of the data. The bandwidth of their power estimates is known, and (subject to this resolution limit) the method shows all peaks in the chosen frequency range of the spectrum, without prior knowledge.

Lines in the spectrum correspond to the magnetic variations of interest here (i.e. periodic variations), and will be referred to as signals; the continuum power corresponds to random magnetic fluctuations and, since it is of no interest here, will be regarded as noise. The investigation of periodic magnetic variations thus concerns the detection and estimation of lines in the

spectrum in the presence of noise, and for such an investigation power spectrum analysis based on the autocorrelation function of the data suffers from several disadvantages. Among these are the lack of a good estimate of probable error to associate with the power estimates (see discussion in §3), the (positive) biasing of the estimates by noise, the possible need to prewhiten the data, the lack of flexibility of the method (separate analyses are performed for each different resolution spectrum, and for all cross-spectra), and the long computing time required.

To overcome the disadvantages of the C.–M. method and of autocorrelation power spectrum analysis, a method of spectral analysis using discrete Fourier transforms is developed here. The use of Fourier transforms was once prohibited by the excessive computing time required, but fast algorithms—apparently first derived (see Cooley, Lewis & Welch 1967) by Runge (1903), but not widely known until rediscovered by Cooley & Tukey (1965)—have removed this objection. The literature on autocorrelation power spectrum analysis is extensive (see, for example, Jenkins 1965; Jenkins & Watts 1963), but little of it is relevant to the approach via Fourier transforms; even the published work that uses Fourier transforms as a tool (reviewed by Hinich & Clay 1968) does not modify the method to overcome the principal disadvantages of auto-correlation power spectrum analysis.

2. DATA USED

The data analysed in this paper consisted of alternate hourly mean values of magnetic West declination (D), measured at Abinger, England (51° 11′ N, 0° 23′ W), in the period 1926–57 (Greenwich Magnetic and Meteorological Observations 1926–57). The values were given to 0.1′, and the first value of each day corresponded to 00.30 U.T. At the dip latitude of Abinger (49° N) periodic variations in the frequency range 0 to 6 c/d are most conspicuous in the declination, so that this magnetic element was chosen for the analyses.

Much theoretical work on time series analysis (see, for example, Blackman & Tukey 1958; Goodman 1957) assumes that the data are both stationary and Gaussian. A time series is stationary if its autocorrelation is a function only of the lag and not of the time origin of the data. Auto-correlations of the Abinger data for various lags showed no systematic change with epoch, and the data are assumed to be stationary.

To define the Gaussian assumption, assume that the time series is generated by a random process, and regard any particular value as being one of an (unobservable) ensemble of values that might have been generated. The time series is Gaussian if the ensemble has a Gaussian distribution; the ensemble cannot be tested, but (under conditions here satisfied) averages across the ensemble are equivalent to time averages along the ensemble. The data contain signals that are not expected to be Gaussian, and it was also found that 5 % of the data points had exceptionally large scatter (presumably these correspond to magnetic storms); the seven largest frequency components and the 5 % of points with large scatter were removed from four thousand points of Abinger data, and a χ^2 test on this modified data showed that there was no reason to reject the hypothesis that the noise part of the data was Gaussian.

3. AUTOCORRELATION POWER SPECTRUM ANALYSIS

The results presented in this section show the main features of the magnetic declination spectrum in the frequency range 0 to 4.5 c/d. The method follows Blackman & Tukey (1958) and the computations were performed with the BOMM (1966) program package. Two lengths of

800 days (9600 points) data were processed, one length at sunspot maximum (6 January 1947 to 15 March 1949) and one at sunspot minimum (4 January 1953 to 14 March 1955). The data were checked for errors, and were corrected by interpolation when first or second differences exceeded 12.0' or 18.0' respectively. This error check altered 0.5 % of the points at sunspot maximum and 0.36 % at sunspot minimum; a more severe first difference limit would have removed power from the solar daily variation peak.

The sampling interval of the data, Δt, was 1/12 day which gives a Nyquist frequency, f_N, of $1/(2\Delta t) = 6 c/d$. The resolution, Δf, was chosen to be 1/300 c/d, which required that the auto-correlation function be calculated at 1800 lags. In general, a pure sinusoidal signal in the data will appear in the spectrum as a band of width $\sim 2\Delta f$ together with sidelobes that decrease in height as $1/\delta f$, where δf is the distance in frequency from the main peak. To reduce this leakage power in the sidelobes, the autocorrelation function was multiplied by a cosine bell lag window $\frac{1}{2}(1 + \cos(\pi l/1800))$, where l is the lag number, before taking the cosine transform of the auto-correlation to obtain the power spectrum. Multiplication by this lag window before transforma-tion is equivalent to smoothing (with weights $\frac{1}{4}$, $\frac{1}{2}$, $\frac{1}{4}$) the spectrum obtained by transforming the original autocorrelation function. This smoothing, somewhat paradoxically, broadens the main peak (to a width $\sim 4\Delta f$) but reduces substantially the leakage power appearing at more than $2\Delta f$ from the centre of the peak. This lag window gives each estimate a bandwidth of $\sim 4\Delta f$, so that at frequency f the power estimate $P(f)$ is influenced by power in the data in the range $f \pm 2\Delta f$.

The data were not prewhitened. Prewhitening is a filtering operation (convolution in time) to flatten the spectrum and so avoid the swamping of a small feature by leakage of power from a nearby large peak. The most common application of prewhitening is in removing low-frequency power from the data; as another example, Leaton et al. (1963) state that they need to remove solar variations from the data in order to evaluate the smaller lunar variations. Prewhitening is only of use because the width of the filter can be less than the bandwidth of an estimate: analysing a record of N points at m lags broadens the natural bandwidth by a factor N/m, and so the removal of a large peak before this blurring takes place will preserve nearby small peaks that would otherwise be swamped. For the present analysis, power leakage was controlled by the use of a lag window and by using sufficient resolution to separate the peaks of interest by several bandwidths.

The data consisted of hourly means, not instantaneous values. The use of means ensures that there is no aliasing (the appearance of power in the computed spectrum at frequencies below f_N that is in reality at frequencies above f_N), but the spectrum must be corrected by multiplication by a slowly varying function of frequency to obtain the true power. This function is (Chapman & Bartels 1940):

$$F(f) = (f\pi/24 \sin(f\pi/24))^2, \tag{3.1}$$

where f(c/d) is the frequency. For $f = 0, 1, 2, 3, 4$ c/d, $F(f) = 1.0, 1.006, 1.024, 1.053, 1.096$ respectively.

The spectra for sunspot minimum and sunspot maximum are similar, but the noise level at sunspot maximum is higher and the peaks are somewhat less prominent. Figure 1 shows sections of the spectrum around 0, 1, 2, 3, 4 c/d for sunspot minimum, and also a section around 1 c/d for sunspot maximum for comparison. Since the ultimate aim of this investigation is to determine the amplitudes of magnetic variations, the normalization of the power spectrum is such that a peak of total power M^2 (i.e. the sum of the power estimates comprising the peak is M^2)
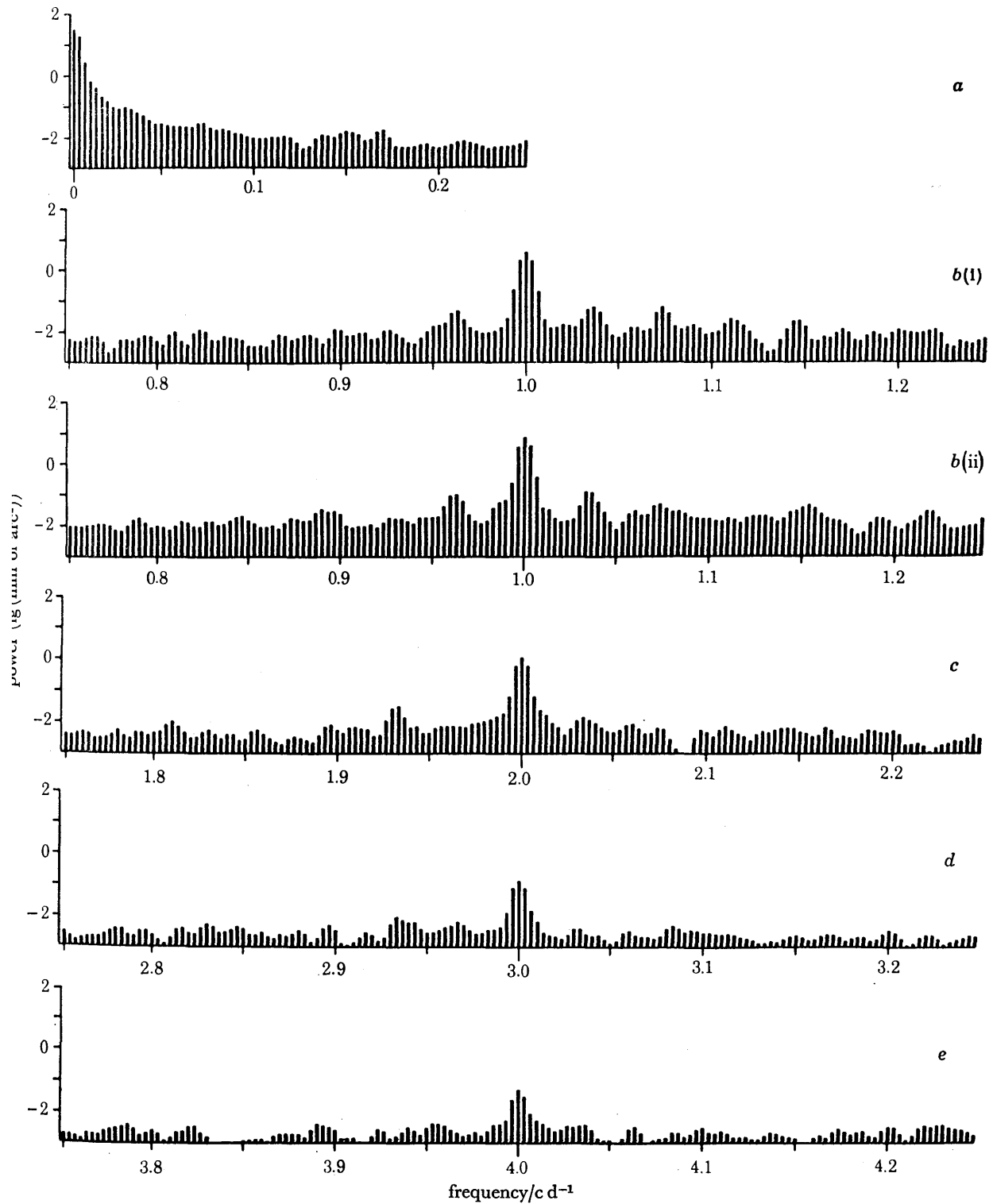
FIGURE 1. Power spectrum of Abinger declination data (spectrum obtained from the autocorrelation function). Panels a, b(i), c, d and e are for data at sunspot minimum, panel b(ii) is for data at sunspot maximum. $\Delta f = 1/300$ c/d; number of data points used = 9600; number of lags = 1800.

corresponds to a magnetic variation $M \cos(2\pi ft)$, and not (as is more usual) to a variation $\sqrt{2} M \cos(2\pi ft)$.

The spectrum shows background noise at all frequencies: the continuum power between the regions shown is roughly constant and equal to the noise power seen in figure 1. Peaks in the spectrum stand above this noise by up to 2.5 orders of magnitude. Using the spectrum alone, one can only deduce the origin of the peaks from their frequency. The largest peaks at 1, 2, 3, 4 c/d are certainly the solar diurnal variation and its harmonics; the peak at $1.932(= 2 - \frac{2}{29})$ c/d is the lunar semi-diurnal variation. The peaks near to 1 c/d, at 0.96, 1.04, 1.07, 1.11, and 1.14 c/d, are unexpected, and it will be seen later that no lunar variations are predicted at these frequencies.

The autocorrelation power spectrum leaves two problems. The first is the presence of the continuum noise, which both biases the power estimates and makes it difficult to detect peaks. It is shown in appendix C (*a*) that the expectation of the total power of a peak is the sum of the signal and the noise power. The noise power, however, fluctuates from one frequency to another, for a given data sample, so that, although in principle one may subtract the continuum power from the total power to obtain the signal power (with the assumption that the noise at the peaks is equal to the adjacent continuum level), in practice this is not possible. The difficulty may be illustrated with the peak at 2.933 c/d. Is this a real peak, or merely a noise fluctuation? If it is a real peak, what is the appropriate noise power to subtract from it?

The second problem is the lack of confidence limits for the power estimates. Blackman & Tukey (1958) give theoretical confidence limits, in terms of degrees of freedom (given by twice the number of data points divided by the number of lags), under the assumptions that the data are Gaussian and that the spectrum is smooth over the spectral window (i.e. the bandwidth) of the estimates. For the spectrum in figure 1, the number of degrees of freedom is *ca.* 11, which gives 80 % confidence limits of 0.5 and 1.6 times the estimate. However, both assumptions cease to be valid at lines in the spectrum, at which points it is claimed (Blackman & Tukey 1958) that the 80 % confidence limits expand to 0.1 and 2.3 times the estimate. From experience, the estimates are considerably more reliable than this, but no quantitative confidence limits are available.

Fourier transforms of many blocks of data will be used in § 6 (by the method to be developed in § 4 (*b*)) to overcome these two problems. Information on the origin of the spectral peaks and the phase of the magnetic variations will also be obtained in § 6, by calculating the coherence and phase between the magnetic data and a theoretical model.

4. FOURIER TRANSFORM ANALYSIS

(*a*) Discrete Fourier transforms

Let the data series, $X(t)$, be given for a time interval $0 \leqslant t \leqslant T$ at N equally spaced points Δt apart, so that $(N-1)\Delta t = T$. For convenience, N is taken to be even. $X(t)$ may be represented exactly at the points $m\Delta t$ in the interval $(0, T)$ by a finite series of orthogonal trigonometric terms:

$$X(t) = \sum_{k=0}^{\frac{1}{2}N} A_k \cos(2\pi kt/T) + \sum_{k=1}^{\frac{1}{2}N-1} B_k \sin(2\pi kt/T). \qquad (4.1)$$

There are other complete sets of orthogonal functions on the straight line; sines and cosines are the natural choice here because the phenomena of interest approximate well sinusoidal

variations. Estimates of the power, $P(f)$, and phase, $\theta(f)$, are obtained at discrete frequencies $f = k/T$ for $k = 0, 1, ..., \frac{1}{2}N$ (i.e. $\Delta f = 1/T, f_N = N/2T$) where

$$P(k/T) = P_k = A_k^2 + B_k^2 \quad [k = (0, \tfrac{1}{2}N)], \qquad (4.2\,a)$$

$$\theta_k = -\tan^{-1}(B_k/A_k) \quad [k = (0, \tfrac{1}{2}N)]. \qquad (4.2\,b)$$

The notation $k = (a, b)$ is introduced to indicate that an integer variable, k, can take all integer values from a to b inclusive.

It is of interest to compare these power estimates with those obtained from the autocorrelation function; the relation is derived in appendix A.
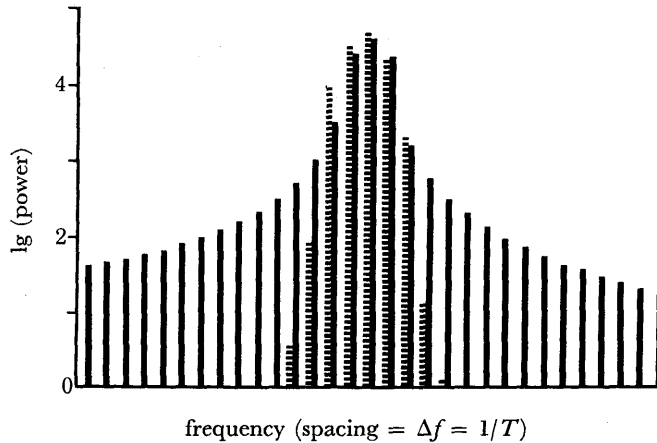

FIGURE 2. Power spectra of a pure sinusoidal signal. Spectra obtained from Fourier transform, with use of cosine bell data window (dashed columns) and without use of data window (plain columns).

To reduce power leakage, the data series is multiplied by a cosine bell data window, $\frac{1}{2}\{1 - \cos(\pi t/T)\}$. This is equivalent to convolving each of the two coefficient series A_k, B_k with weights $-\frac{1}{4}, \frac{1}{2}, -\frac{1}{4}$ before calculating P_k. The reduction in leakage achieved by this window is shown in figure 2. This data window reduces the power estimates by a factor $\frac{3}{8}$, so the spectrum must be corrected for this.

(b) Estimates of amplitude unbiased by noise

If there is noise in the data, each Fourier power estimate P_k will have low stability, i.e. estimates at the same frequency from different epochs of data will have a large scatter. The stability may be improved by smoothing the estimates. The data may be postwhitened before smoothing: the power spectrum obtained from the Fourier transform shows peaks with their natural bandwidth (for a length T of data and for a sinusoidal signal, this natural width is ca. $2/T$), and to avoid power spreading sideways from peaks during the smoothing process, the peaks may be set equal to the adjacent power level before smoothing, and replaced subsequently. This post-whitening is much quicker, more accurate and easier (since the spectrum is known) than the prewhitening required, before calculation of the power spectrum from the autocorrelation function, to achieve the same ends.

Smoothing the power estimates implies a loss of resolution, and the estimates are no longer independent, but the smoothed spectrum is essentially the same as that obtained by the auto-correlation method at the equivalent resolution.

Stability may alternatively be improved by splitting the data into several, say p, sections,

calculating Fourier power estimates for each, and combining the p estimates at each frequency to give a 'best' estimate. This procedure may be used with blocks of data that are not consecutive, and one can combine the p estimates in such a way that the best estimate is not biased by noise (i.e. the presence of noise at the same frequency as the signal no longer increases the expected value of the estimate), while confidence limits for the best estimate may be obtained. In this procedure, developed below, it happens to be more convenient to work with the amplitudes of the Fourier transform rather than the power, i.e. to use $\sqrt{P_k}$ rather than P_k, and the method then gives an amplitude spectrum and not a power spectrum; the difference is trivial, except that peaks in the spectrum are less conspicuous in amplitude than in power.

At a specific frequency k/T, let the Fourier transforms of the p blocks of data be

$$R_j = A_j + iB_j = R_j \exp(i\theta_j) \quad [j = (1, p)], \tag{4.3}$$

where the dependence of all variables on k is understood.

Let the Fourier transforms of the signal be $S_j = S \exp(i\phi_j)$, where the amplitude S of the signal is assumed constant for all j, and let the Fourier transforms of the noise by $N_j = N_j \exp(i\psi_j)$. Then we have

$$R_j \exp(i\theta_j) = S \exp(i\phi_j) + N_j \exp(i\psi_j) \quad [j = (1, p)]. \tag{4.4}$$

For the first block of data, the Fourier transform of the signal is $S \exp(i\phi_1)$. It is natural to expect that, if ΔT_q is the time interval between the initial points of the first and qth blocks of data, then ϕ_q will be given by

$$\phi_q = \phi_1 + 2\pi k \Delta T_q / T. \tag{4.5}$$

It thus appears that $\phi_q - \phi_1$ is a known quantity, and we have

$$R_q \exp(i[\theta_q - \phi_q + \phi_1]) = S \exp(i\phi_1) + N_q \exp(i[\psi_q - \phi_q + \phi_1]), \tag{4.6}$$

so that by rotating the qth Fourier transform of the data by $-(\phi_q - \phi_1)$ the signal for each block of data will be in phase, while the noise phases will be random. However, this procedure cannot be followed; it is shown in appendix B (b) that in the absence of noise the phase of an estimate changes by $2\pi(k + \delta k) \Delta T_q / T$ between the first and qth blocks of data, where k/T is the frequency of the estimate and $(k + \delta k)/T$ is the (unknown) frequency of the signal. The discrete Fourier transform cannot define the frequency of a signal to better than $\delta k \simeq \frac{1}{2}$; the required phase change to bring the signal from each block of data into phase cannot therefore be made.

As there is apparently no way to add the signal in phase, the phase information must be discarded, and S must be obtained from the p amplitudes R_j.

It is plausible to assume that the vectors N_j have a Rayleigh distribution, i.e. in polar coordinates the probability of a vector lying in an area $r \, d\theta \, dr$ is $(h^2/\pi) \exp(-h^2 r^2) \, r \, d\theta \, dr$. It is shown in appendix C(a) that under this assumption the amplitudes R_j have the probability density function

$$P(R) = 2h^2 \exp(-h^2[R^2 + S^2]) I_0(2h^2 RS), \tag{4.7}$$

where I_0 is the zero-order modified Bessel function.

The shape of this distribution is shown in figure 5, for various values of the parameters. From the sample of p points R_j from this distribution one may obtain estimates $\hat{S}, \hat{h}$ for the parameters S and h. 'Best' estimates (in many senses) may be found by the method of maximum likelihood (Kendall & Stuart 1967) which gives implicit equations for $\hat{S}, \hat{h}$:

$$\sum_j (R_j^2) = p(\hat{S}^2 + 1/\hat{h}^2), \tag{4.8}$$

$$\sum_j R_j I_1(2\hat{h}^2 R_j \hat{S}) / I_0(2\hat{h}^2 R_j \hat{S}) = p\hat{S}. \tag{4.9}$$

These equations give unbiased estimates of S and h (appendix C (b)). Maximum likelihood estimates of two parameters tend, for large p, to be distributed in bivariate normal form, and the standard deviation σ_S, σ_h of the estimates of S and h, as well as their covariance σ_{Sh}, may be found from the R_j. It may be shown that no other estimates that are unbiased and normally distributed for large p can have smaller variance than the maximum likelihood estimates.

The method used to obtain the estimates of S and h given by equations (4.8) and (4.9), and the equations for σ_S, σ_h and σ_{Sh}, are given in appendix C (c), (d).

(c) Calculation of coherence and phase

The Fourier transforms of two time series that have the same start time, sampling interval, and end time enable the coherence and phase between the two series to be obtained with little further computation. No cross-spectral analysis is required, since the two Fourier transforms define the cross-spectrum as well as the individual power spectra.

To obtain meaningful estimates of coherence and phase, the two series must be split into many, say p, equal sections. Let the Fourier estimates at a particular frequency k/T be X_j, Y_j, $j = (1, p)$. The coherence γ^2 at this frequency is then

$$\gamma^2 = |\sum_j X_j Y_j^*|^2 / (\sum_j X_j X_j^*) (\sum_j Y_j Y_j^*) \tag{4.10}$$

and

$$0 \leqslant \gamma^2 \leqslant 1.$$

If no averaging over many sections is performed, i.e. if the Fourier transforms of the two entire series are used, then $\gamma^2 \equiv 1$. The power spectrum obtained from the Fourier transform of one length of data is almost meaningless because of the large scatter of points; coherence estimates using only one length of data from each series are meaningless because there is no scatter.

The phase between the two series, Θ_{XY}, is

$$\Theta_{XY} = \tan^{-1}\{\mathrm{Im}\,(\sum_j X_j Y_j^*) / \mathrm{Re}\,(\sum_j X_j Y_j^*)\}, \tag{4.11}$$

Θ_{XY} is the phase lead of series X with respect to series Y.

It may be shown that the estimate of phase Θ_{XY} is unbiased, but the coherence γ^2 is (positively) biased by noise (Munk & Cartwright 1966, appendix B). Munk & Cartwright show that the quantity $(p\gamma^2 - 1)/(p - 1)$ is an approximately unbiased estimate of the true coherence. Munk & Cartwright (1966) give confidence limits for Θ_{XY} as a function of a noise parameter

$$\sigma = ((\gamma^{-2} - 1)/2p)^{\frac{1}{2}}.$$

Foster & Guinzy (1967) show the probability distribution of the true coherence for various values of the sample coherence γ and p. This paper follows Foster & Guinzy (1967) in using γ as the measure of coherence rather than γ^2.

5. MODEL OF LUNAR AND SOLAR MAGNETIC VARIATIONS

Matsushita (1967) has reviewed the literature on the solar quiet and lunar daily variation fields. The predominant magnetic variations in the frequency range 0 to 4 c/d have periods related to the lunar and solar periods. These variations are caused by atmospheric tides. The tidal motion of the conducting layers of the ionosphere relative to the main geomagnetic field creates ionospheric currents which are observed at the Earth's surface as magnetic variations.

Matsushita (1967) concludes that, contrary to earlier opinion, the current systems responsible for the lunar (L) variations and the solar quiet day (S_q) variations flow in the same layer, the E layer (height *ca.* 80 to 170 km), of the ionosphere.

The Moon can raise only a gravitational tide in the atmosphere: the magnitude at Greenwich $(51°29'N, 0°00'W)$ of the lunar semi-diurnal tide is $1.2\,\mu$bar (Haurwitz & Chapman 1967). This tide is 2.5 times greater than the pressure fluctuation of an atmosphere in equilibrium with the lunar gravitational field. The ratio of the Moon's tidal force on the Earth to that of the Sun is approximately 2.4, but while this is the observed ratio of lunar and solar ocean tides, the solar semi-diurnal atmospheric tide is far greater than the lunar tide. The solar tide is magnified 90 times relative to the equilibrium tide: this was long thought to be a resonance effect, but it has now been shown that the solar tide is thermally excited by atmospheric absorption of solar radiation (Siebert 1961; Butler & Small 1963).

The ionosphere is rendered conducting by solar radiation. The conductivity is anisotropic, and different components are dominant at different heights, but for a first approximation it may be assumed that the conductivity is proportional to the incident radiation.

No further inquiry into the ionospheric process producing the magnetic variations is needed here, and the variations may simply be regarded as the output from a complex physical system. Magnetic variations are the result of a multiplicative interaction between tidal motions and ionospheric conductivity; thus a simple model for the input to the system for lunar variations is the product of lunar gravitational potential and solar radiation, while for a model of the input function that gives rise to solar variations the square of solar radiation suffices and the contribution of solar gravity may be neglected. It is expected that lunar and solar variations will be present in the spectrum of magnetic records at only those frequencies at which there are peaks in the spectra of input functions.

At a given point on Earth, the magnetic variations depend on the spatial configurations of the tides and conductivity variations in the vicinity of that point. To predict magnetic variations, the tides and conductivity variations must be analysed into spherical harmonies, and each interacting pair of spherical harmonies must be multiplied by a different factor to give its contribution to the total magnetic variation. No such spatial analysis is attempted here. The lunar and solar time series used to form the model input functions are the total lunar equilibrium tide and the total incident solar radiation at Abinger. This implies that no significance can be attached to the exact ratio between corresponding peaks in the spectra of the magnetic data and the input functions.

The observed data are better compared with the models by calculating the coherence and phase between the series. A high value of coherence is an indication (but in no sense a proof) that at that frequency the modelled process is the cause of the magnetic variation. The coherence is normalized so that it is independent of the relative magnitude of the power in the two series. The estimate of phase between the series is the true phase between the magnetic variation and the input function.

6. Results of Abinger analysis

The amplitude spectrum of Abinger declination was obtained from the Fourier transforms of seventeen epochs of data, each of length 4096 points ($341\frac{1}{3}$ days). The epochs are listed in table 1, together with an average sunspot number for each epoch. The seventeen epochs sample all parts of the sunspot cycle, so that the assumption that the signal is constant from epoch to epoch is

violated; however, the signal fluctuation with the sunspot cycle may be regarded as noise, and the signal amplitude obtained will be an average over the sunspot cycle.

Errors in the data were corrected by interpolation, as discussed in § 3, and each epoch of data was multiplied by a cosine bell data window and Fourier transformed. The frequency interval is $\Delta f = 1/341\frac{1}{3} = 0.00293$ c/d, and at each frequency $k\Delta f$ the seventeen Fourier amplitudes were used to estimate the amplitude S of the magnetic variations, and the standard deviation σ_s of $\hat{S}$, by the method described above in § 4 (b).

TABLE 1. EPOCHS OF DATA USED TO OBTAIN THE AMPLITUDE SPECTRUM OF
ABINGER DECLINATION

epoch	sunspot number	epoch	sunspot number
1 Jan. 1927–8 Dec. 1927	69	28 July 1946–4 July 1947	122
8 May 1928–14 Apr. 1929	74	5 Aug. 1947–10 July 1948	144
15 Apr. 1929–22 Mar. 1930	55	1 Jan. 1951–8 Dec. 1951	69
17 Aug. 1930–25 July 1931	26	9 Dec. 1951–14 Nov. 1952	32
26 Jan. 1932–1 Jan. 1933	11	15 Nov. 1952–22 Oct. 1953	14
4 Jan. 1933–11 Dec. 1933	5	23 Oct. 1953–29 Sept. 1954	4
15 Feb. 1935–22 Jan. 1936	36	30 Sept. 1954–6 Sept. 1955	27
23 Jan. 1936–29 Dec. 1936	79	7 Sept. 1955–13 Aug. 1956	107
2 Jan. 1945–9 Dec. 1945	33		

The estimates of S are normally distributed if the number of sample points p used to obtain $\hat{S}$ at each frequency is large. This analysis used seventeen epochs of data giving seventeen values of R_j at each frequency; seventeen is not a large sample, but it is sufficient for the estimates of σ_s to give a good indication of the reliability of the values of $\hat{S}$.

The top panels of figure 3 (a), (b), (c), (d) and (e) show the amplitude spectrum and standard deviation of the amplitude estimates for frequency ranges around 0, 1, 2, 3, 4 c/d. There is no signal shown at those frequencies at which either the maximum likelihood equations (4.8) and (4.9) had only the solution $\hat{S} = 0$, or at which the signal was not significant at the 95 % level (i.e. $\hat{S} \leqslant 1.96\sigma_s$).

A particular magnetic variation, say the solar diurnal variation, will give a significant signal at several adjacent frequencies. The amplitude of the magnetic variation is $(\Sigma S_k^2)^{\frac{1}{2}}$ where the sum is over the estimates comprising the peak. Thus the solar diurnal variation has an amplitude of $(0.28^2 + 0.78^2 + 2.36^2 + 1.77^2 + 0.41^2)^{\frac{1}{2}} = 3.09'$. The standard deviation of each estimate is known, and the probable error, δS, of the magnetic variation may be taken as (Topping 1955)

$$\delta S = \left\{ \frac{\Sigma \hat{S}_k^2 \sigma_{Sk}^2}{\Sigma \hat{S}_k^2} \right\}^{\frac{1}{2}}. \tag{6.1}$$

Thus the probable error of the solar diurnal variation is $0.1'$. The conversion between units of minutes of arc and gammas for declination at Abinger is 5.4γ/min (Leaton et al. 1963), which gives an alternative expression for the solar diurnal variation of $16.7 \pm 0.5\gamma$. ($1\gamma = 10^{-5}$ G = 10^{-9} T = $1n$T.)

I am indebted to Dr W. H. Munk for supplying me with time series of lunar gravitational potential, solar gravitational potential and incident solar radiation at Abinger for the last six epochs of table 1 (1 Jan. 1951 to 13 Aug. 1956). The lower six panels of figure 3 show the spectrum of the lunar input function (lunar gravity times solar radiation), the coherence and phase between the lunar input and Abinger data, the spectrum of the solar input function (solar radiation squared), and the coherence and phase between the solar input and Abinger data. The

FIGURE 3 (*a*) to (*e*) (see pp. 244 to 248). The top panel is the amplitude spectrum of Abinger declination data; the bar across each column is the height of the standard deviation of the estimate of amplitude. Amplitudes greater than 0.2′ are shown numerically. The second, third and fourth panels show the lunar input spectrum, and the coherence and phase between Abinger data and the lunar model. The fifth, sixth and seventh panels show the solar input spectrum, and the coherence and phase between Abinger data and the solar model. The phases are the phase lags of Abinger data with respect to the input models. $\Delta f = 0.00293$ c/d.
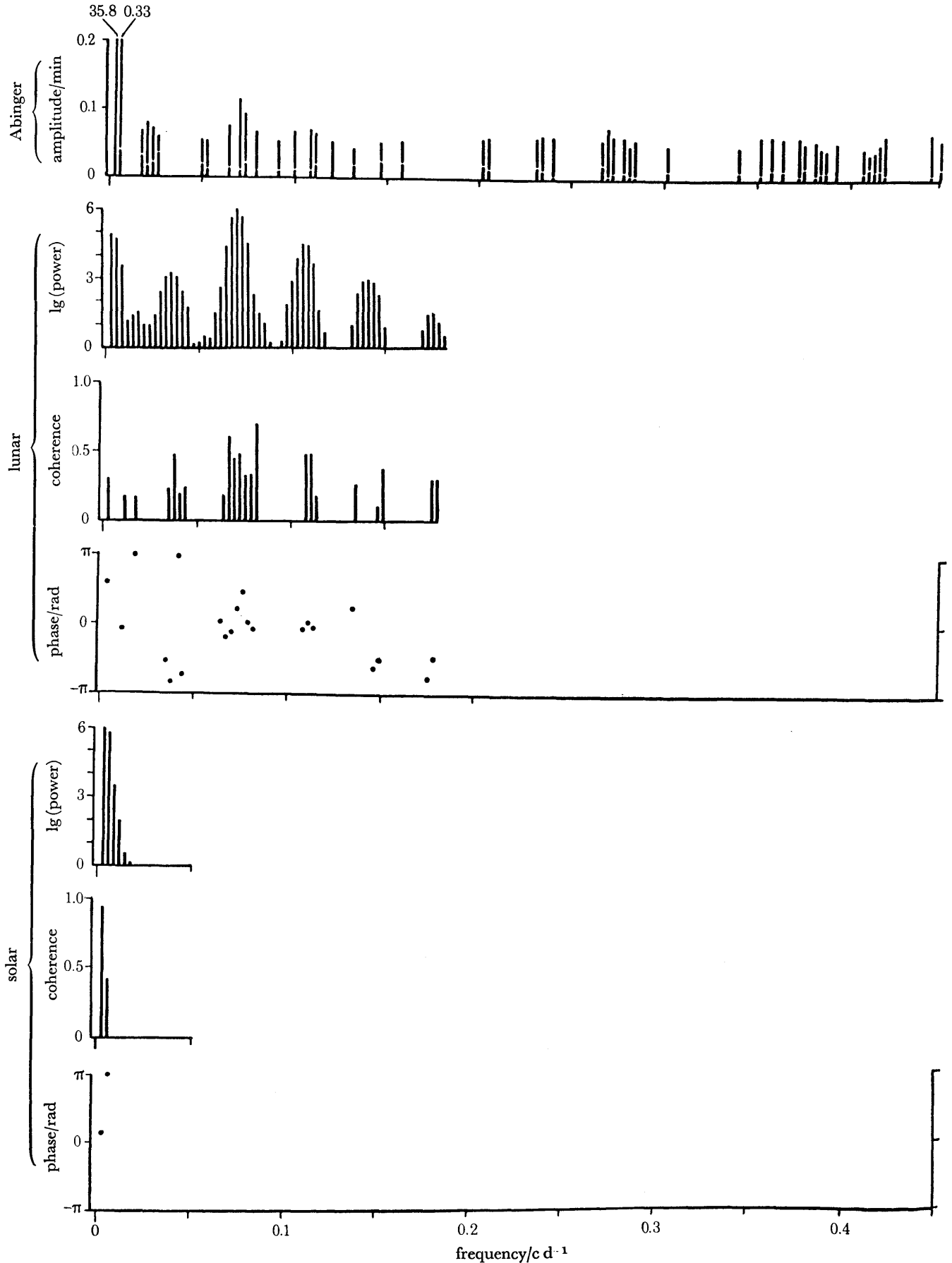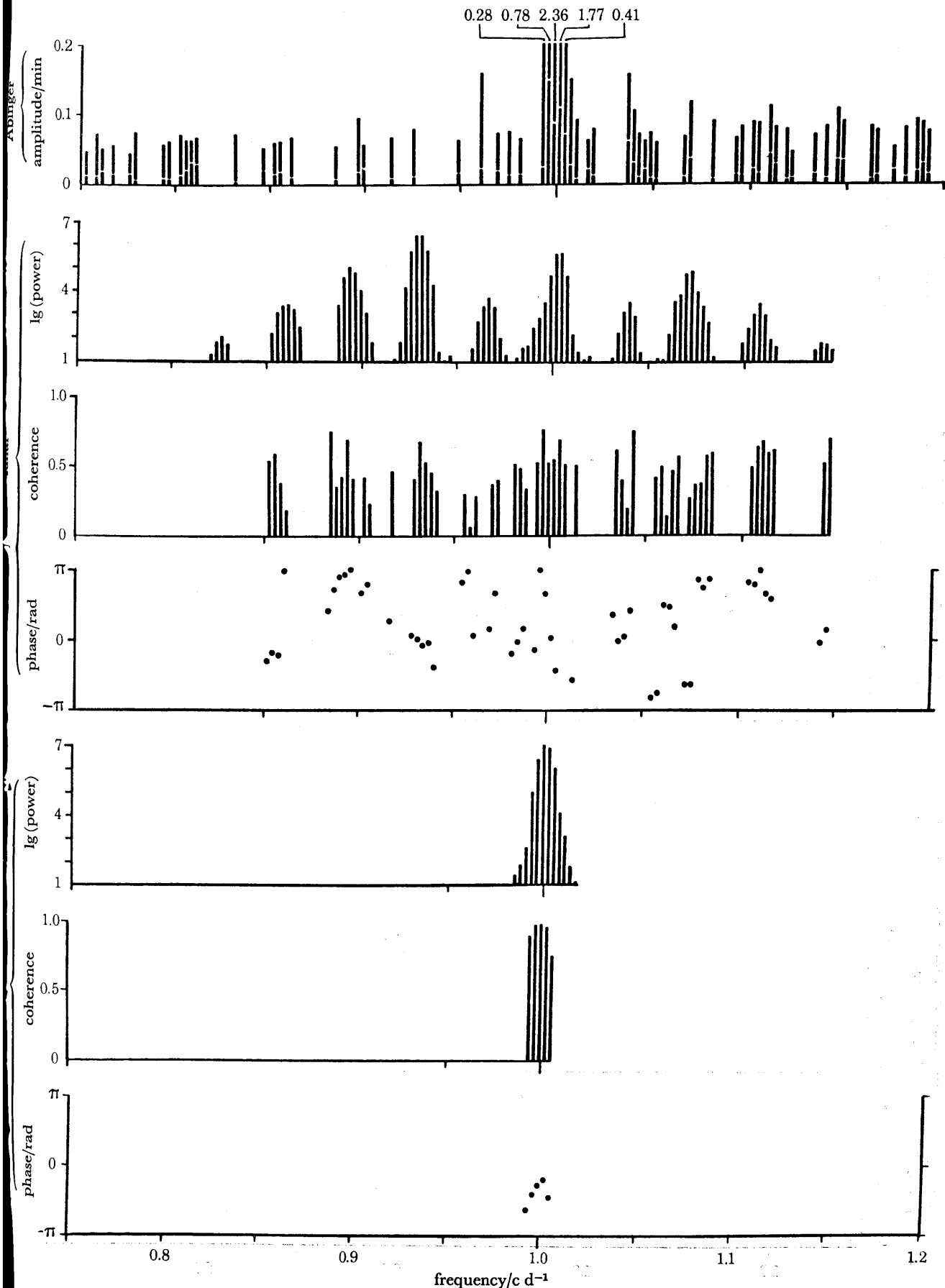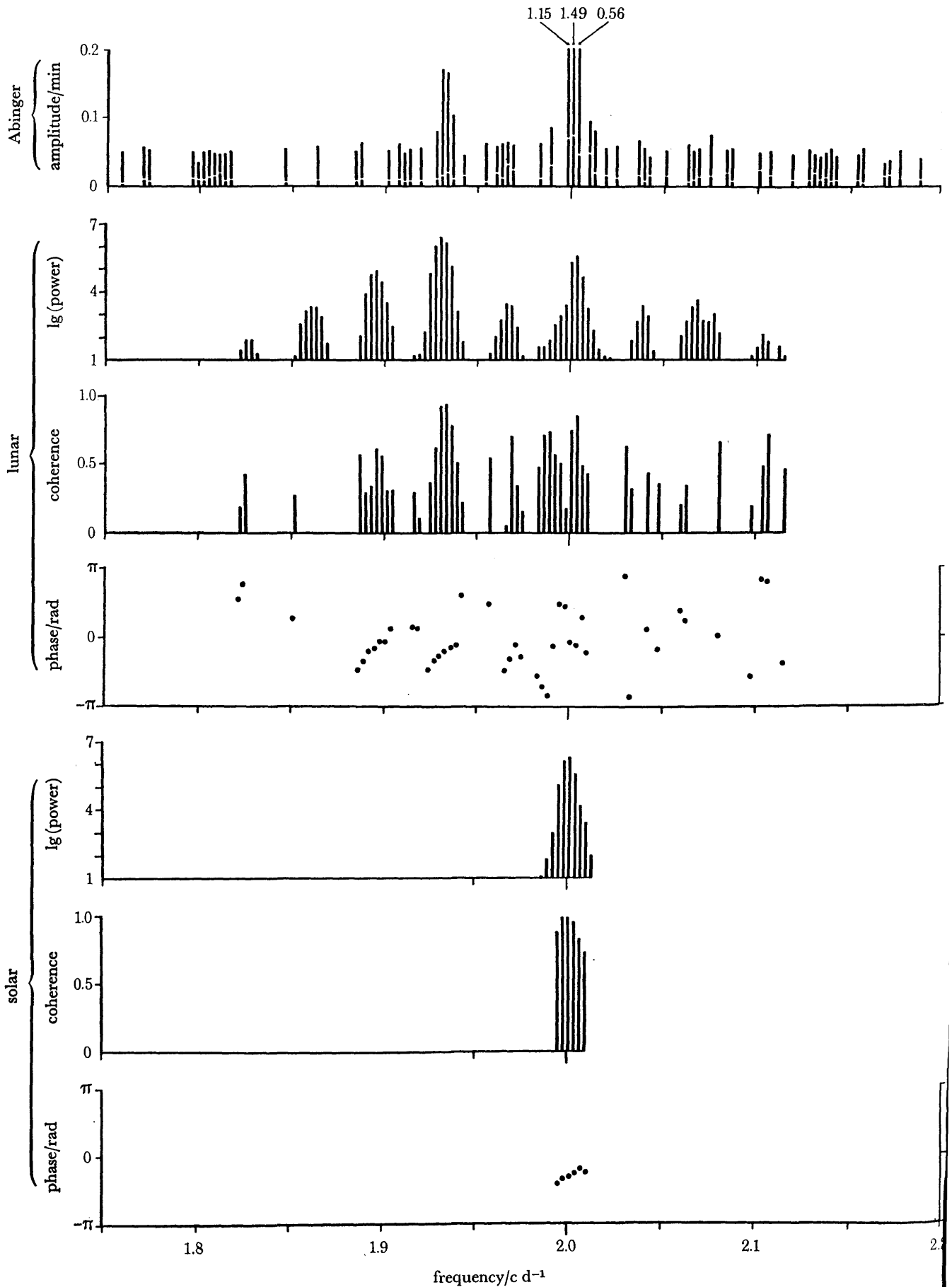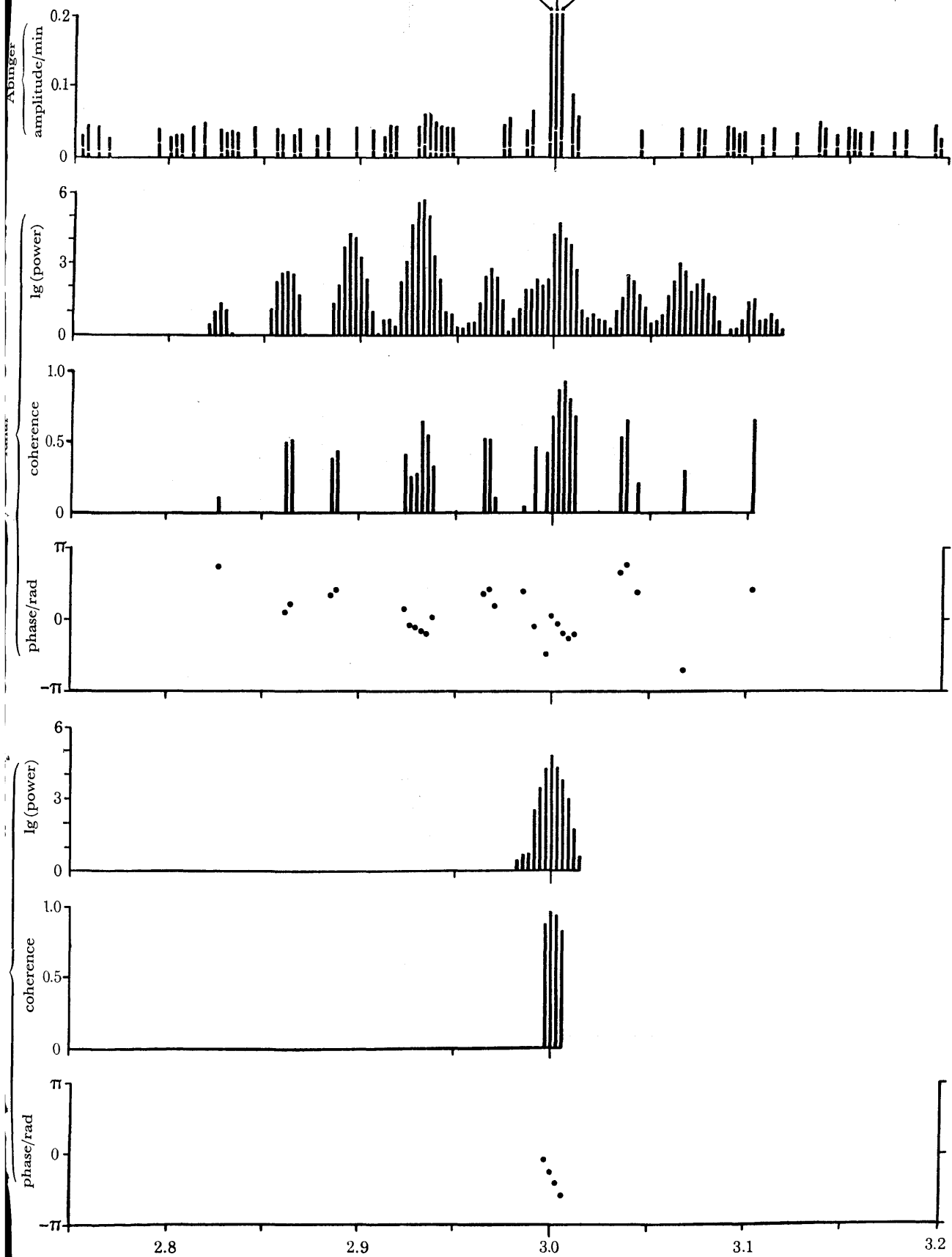

FIGURE 3 (*a*)

0.28 0.78 2.36 1.77 0.41
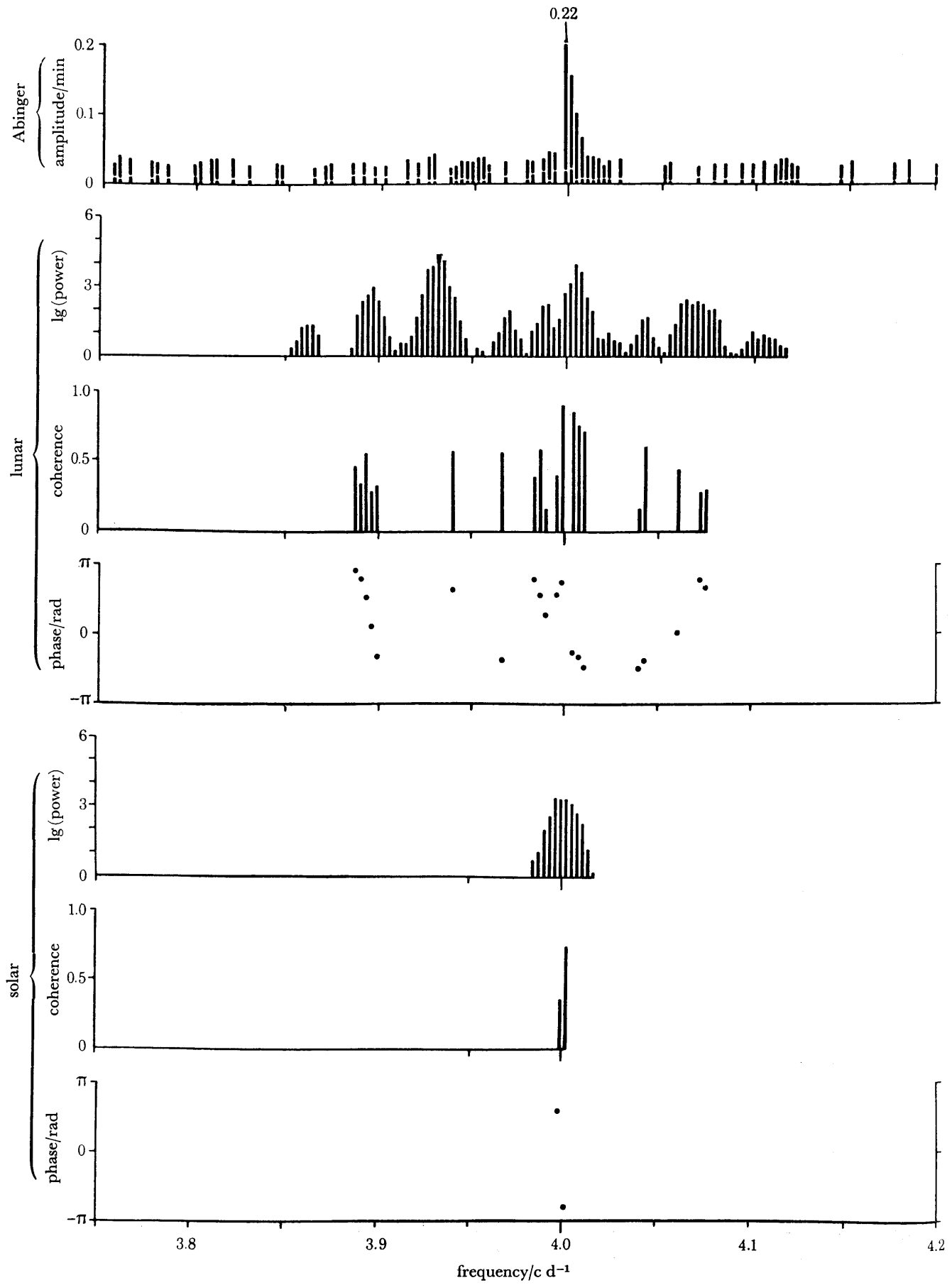
FIGURE 3 (b)

FIGURE 3(c)

FIGURE 3 (d)

D. I. BLACK

FIGURE 3 (e)

spectrum of the product of solar gravitational potential and solar radiation (i.e. a model for gravitationally excited solar variations) was also calculated, but no frequencies other than those in the spectrum of (solar radiation)^2 were present; this is to be expected since both solar gravity and radiation contain only frequencies that are integral multiples of 1 c/d, apart from annual variations.

The frequencies of the major solar and lunar tides (i.e. the lines in the spectra of solar and lunar gravity) are shown in table 2, based on Doodson (1922).

TABLE 2. PREDOMINANT SOLAR AND LUNAR TIDES (DOODSON 1922)

origin (solar or lunar)	symbol	amplitude, A (relative)	argument, Ω	frequency (c/d)	
L	Mm	3 389	$s-p$	$1/27.55$	$= 0.03629$
L	Mf	6 423	$2s$	$1/13.66$	$= 0.07320$
L	O_1	36 814	$\tau-s$	$1-1/14.19$	$= 0.92954$
S	P_1	17 147	$t-h$	$1-1/365$	$= 0.99726$
{ L	K_{1m}	35 392	$\tau+s$	$1+1/365$	$= 1.00274$ }
{ S	K_{1s}	16 427	$t+h$	$1+1/365$	$= 1.00274$ }
L	N_2	6 832	$2\tau-s+p$	$2-1/9.6$	$= 1.89598$
L	M_2	35 682	2τ	$2-1/14.8$	$= 1.93227$
S	S_2	16 615	$2t$	2	$= 2.00000$

The arguments are:

τ = local mean lunar time, increasing by $360° - 12°.1907$ per solar day,
s = Moon's mean longitude, increasing by $13°.1764$ per solar day,
h = Sun's mean longitude, increasing by $0°.9856$ per solar day,
p = longitude of Moon's perigee, increasing by $0°.1114$ per solar day
$(t$ = local mean solar time, increasing by $360°$ per solar day.)

N.B. $360/12.19 = 29.53$; $360/0.9856 = 365.26$; $12.19+0.98 = 13.17$.

These are related by

$$\tau+s = t+h = \text{sidereal time.}$$

The components of the tidal potential are given by

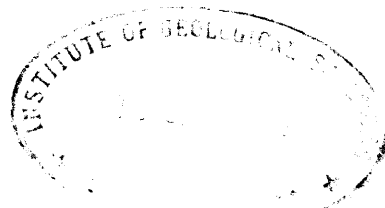$$A \times 10^{-5}\, G \sin \Omega t$$

where A is the relative amplitude (column 3), G a gravitational constant (Doodson 1922), Ω the argument (degrees/solar day), and t the time (solar days).

(a) Section of spectrum 0 to 0.45 c/d

The amplitudes at zero frequency of the Abinger and input spectra are zero because the mean of each epoch of data was made zero before Fourier transformation, for all three series. The peaks in the three spectra at the second and third estimates are caused by slow (i.e. periods of 1 year or more) trends in the data and are of no concern here. The highest remaining amplitude in this region of the Abinger spectrum is at 0.0703 c/d, the frequency of the main peak in the lunar input spectrum: this peak is the lunar semi-monthly line, which results from the interaction of the lunar semi-monthly tide (Mf, see table 2) with the mean conductivity (the reason for the displacement of the Abinger and lunar input peaks by one frequency interval from the expected frequency of 0.0732 c/d is unknown). Although there is no high value of coherence at this frequency, there is little doubt that this peak in the Abinger spectrum is a lunar variation; its amplitude is 0.15'. The autocorrelation power spectrum (figure 1), also shows a ripple on the continuum level at 0.07 c/d—the power in this peak corresponds to a variation of amplitude 0.7', i.e. the power estimates are heavily biased by noise.

No other lunar or solar variations appear in the Abinger spectrum in this region.

(b) Section of spectrum 0.75 to 1.2 c/d

The Abinger spectrum shows a prominent peak at 1 c/d, and both lunar and solar input spectra have peaks at this frequency, but the absence of any other large peaks in this region of the Abinger spectrum indicates that the 1 c/d magnetic variation is almost purely of solar origin. There is no peak in the Abinger spectrum corresponding to the main lunar peak at 0.93 c/d, and no such peak shows in the autocorrelation spectrum (figure 1), or in the high resolution spectrum to be presented in § 7 (figure 4), yet Leaton *et al.* (1963) find a variation of amplitude 0.095′ at this frequency. A lunar magnetic variation of frequency *ca.* 0.93 c/d would arise both from the lunar diurnal tide (O_1) interacting with the mean ionospheric conductivity, and from the lunar semi-diurnal tide (M_2) interacting with the solar diurnal variation of conductivity; the lunar diurnal tide has not been detected in the atmosphere (Lindzen 1967), but the latter contribution should be readily detectable, and no explanation is offered for this missing line.

Since no lunar line at 0.93 c/d appears in the Abinger spectrum, what little correspondence there is between lunar input and Abinger peaks at 1.037, 1.069, 1.11 and 1.146 c/d is almost certainly coincidental. There is also no solar or lunar input peak to account for the Abinger line at 0.961 c/d. The regularity, and the asymmetry, of these sidebands (which were noted before in the discussion of the autocorrelation spectrum) cannot be explained by the lunar or solar models used here. These sidebands of the 1 c/d line are discussed further in § 6 (*f*).

(c) Section of spectrum 1.75 to 2.2 c/d

The two prominent Abinger peaks are at 1.932 and 2.0 c/d, which are the lunar and solar semi-diurnal frequencies. Although both input spectra have peaks at 2 c/d, as before the magnetic variation must be attributed to solar causes. The lunar semi-diurnal variation is the largest lunar variation present in magnetic records; its amplitude at Abinger is 0.24′, and the coherence between the lunar model and Abinger data has the exceptionally high value of 0.9_3. The power in the third largest lunar peak, at 1.89 c/d, is at most one-twentieth of the power of the lunar semi-diurnal peak, so the absence of a corresponding peak in the Abinger spectrum is not unexpected.

(d) Section of spectrum 2.75 to 3.2 c/d

The solar terdiurnal magnetic variation is prominent. There is coherence of 0.6 between a slight peak in the Abinger spectrum and the main lunar peak at 2.931 c/d: as already noted, this peak appears in the autocorrelation spectrum (figure 1), but it may now be identified as a magnetic variation and not a noise fluctuation.

(e) Section of spectrum 3.75 to 4.2 c/d

Only the harmonic of the solar daily variation shows in this region. There is a very slight rise in the Abinger spectrum at the main lunar frequency of 3.932 c/d, but the coherence is zero there.

In table 3 the amplitudes and phases of the main lunar and solar magnetic variations are listed, together with the amplitudes found by Leaton *et al.* (1963) using the Chapman–Miller method. There is excellent agreement between the results obtained by the two methods.

Leaton *et al.* (1963) also searched for lunar magnetic variations produced by the lunar diurnal tide which they assume to have a frequency of 1.932/2 = 0.966 c/d. However, the principal peak in this region of the lunar gravity spectrum is at 0.930 c/d (see table 2), so their negative results are explained.

The smallest magnetic variation listed has an amplitude less than the precision of the data

(0.1′). In the presence of noise, signals of amplitude less than the unit of measurement may be detected, i.e. noise increases the sensitivity of a digital measuring device. Given a sufficient length of data, there is no lower limit to the amplitude that can be detected.

TABLE 3. THE PRINCIPAL SOLAR AND LUNAR MAGNETIC VARIATIONS PRESENT IN
ABINGER DECLINATION DATA

frequency (c/d)	amplitude (min of arc)	phase lag of Abinger (deg)	Leaton et al. amplitude (min of arc)
0.702	0.15 ± 0.02	4 ± 60	—
1.0	3.09 ± 0.10	-43 ± 7	2.91
1.932	0.24 ± 0.02	-44 ± 10	0.23
2.0	1.96 ± 0.14	-60 ± 5	1.88
2.935	0.09 ± 0.004	-33 ± 50	0.074
3.0	0.80 ± 0.03	-46 ± 7	0.79
4.0	0.27 ± 0.02	140 ± 60	0.30

(f) Sidebands of the 1 c/d line

The lunar and solar models satisfactorily explain all lines in the Abinger spectrum except the sidebands of the 1 c/d peak at $1 + 0.037n$ c/d, $n = -1, +1, 2, 3, 4$. The frequency $0.037 = \frac{1}{27}$ suggests a mechanism related to solar rotation.

Owing to the Sun's rotation of approximately 27 days there is a 27-day recurrence tendency in magnetic storms. A strong 27-day periodicity in magnetic activity indices is well established (see, for example, Shapiro & Ward 1966) and, since there is an increase in the solar diurnal magnetic variation with increasing magnetic activity (Leaton et al. 1963), there will be a 27-day period modulation of the solar diurnal magnetic variation.

The solar rotation presumably influences the solar diurnal magnetic variation by the same mechanism as the sunspot cycle, i.e. through a change in ionospheric conductivity. The 1 c/d line in the Abinger spectrum is principally generated by the interaction of the solar diurnal tide with the mean conductivity; the $1 \pm \frac{1}{27}$ c/d sidebands therefore imply a 27-day period modulation of the mean ionospheric conductivity.

If this is the true mechanism, then similar sidebands of the 2 c/d line are expected. No prediction of the relative magnitudes of the two sets of sidebands can be made, so that the absence of sidebands at $2 \pm 0.037n$ c/d does not disprove the solar rotation mechanism.

The lunar semi-diurnal magnetic variation (1.932 c/d) arises from the lunar semi-diurnal tide and the mean ionospheric conductivity, and so this lunar line would be expected to show sidebands at 1.932 ± 0.037 c/d. However, the sidebands of the 1 c/d line have an amplitude less than $\frac{1}{10}$ that of the 1 c/d line itself, and lines $\frac{1}{10}$ of the amplitude of the lunar peak (i.e. ca. 0.02′) would be undetectable.

Harmonics of the 27-day solar rotation effect would produce lines at $1 \pm k/27$ c/d, $k = 2, 3, 4, \ldots$. Such lines are seen only above 1 c/d, and this asymmetry is not predicted by any model requiring low frequency (e.g. $\frac{1}{27}$ c/d) modulation. The lunar magnetic variations appear as asymmetric sidebands of the solar lines only because the lunar frequencies are high, i.e. close to 1, 2 c/d.

7. HIGH RESOLUTION POWER SPECTRUM

Banks (1968) has found a peak at a frequency of approximately $\frac{1}{27}$ c/d in the spectrum of Abinger horizontal and vertical magnetic data. Banks attributes this line to the recurrence tendency of magnetic storms, and supports this view by demonstrating that the observed width
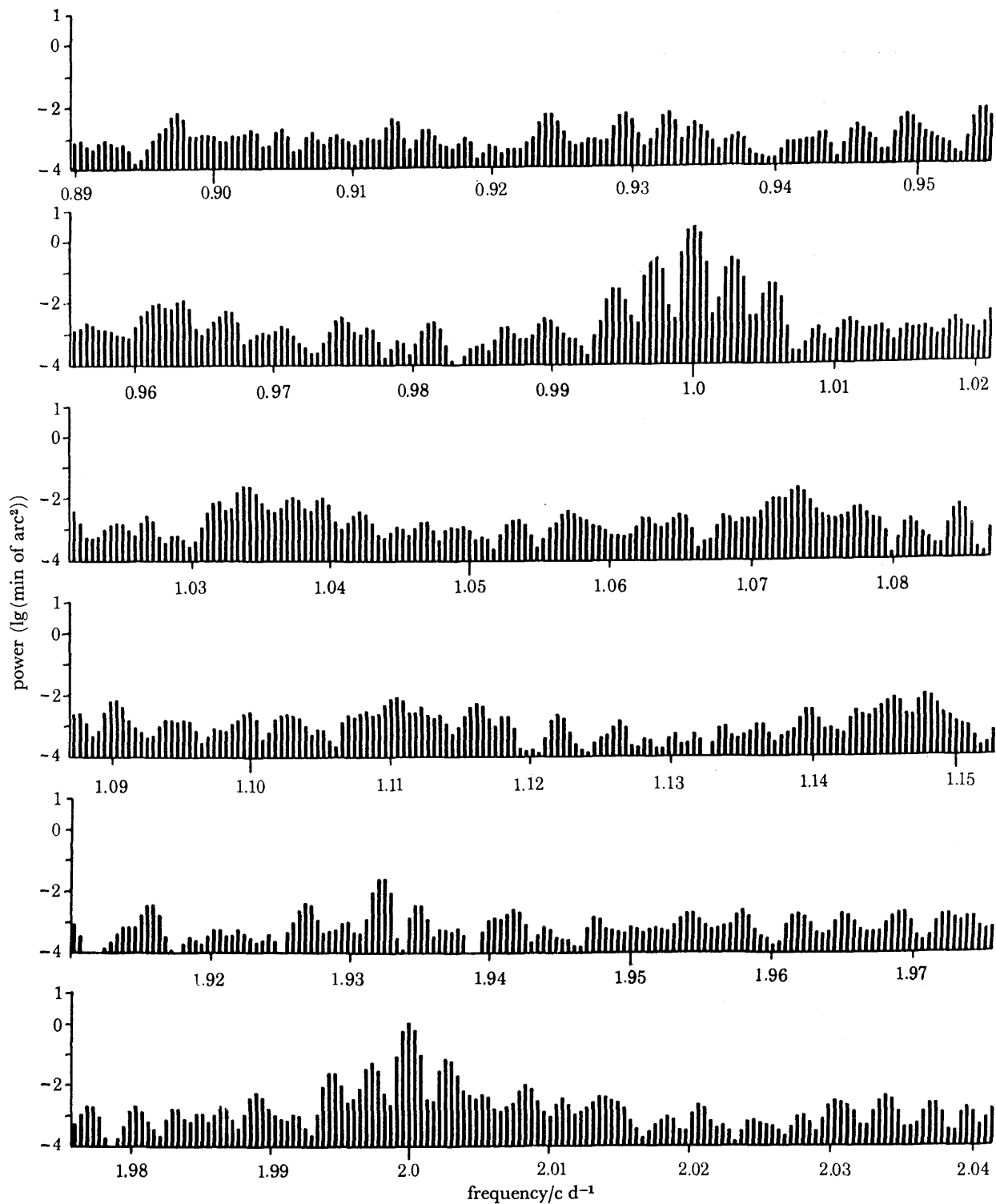
FIGURE 4. High resolution, low stability spectrum of Abinger declination data (spectrum obtained from the Fourier transform). Noise has not been removed from the estimates. $\Delta f = 0.000493$ c/d.

of the line (*ca.* 0.009 c/d) agrees well with simple models of magnetic storms. The large width is due to the finite number (up to about six) of recurrences of a given storm before it disappears, and the irregular occurrence of solar active regions that are the cause of storms.

To determine whether the sidebands of the solar diurnal line in the Abinger declination spectrum may reasonably be attributed to the solar rotation mechanism, a high resolution spectrum was computed. Six years of Abinger declination data (27 360 points, 1 Jan. 1951 to 29 Mar. 1957) were multiplied by a data window and Fourier transformed. The square of the Fourier transform was smoothed with weights $\frac{1}{4}$, $\frac{1}{2}$, $\frac{1}{4}$ to reduce the fluctuations of the estimates (which contain noise and signal power) without losing too much resolution. In figure 4 the spectrum from 0.89 to 1.15 c/d and from 1.91 to 2.04 c/d is shown.

The peaks are inconspicuous because of the very extended horizontal scale ($\Delta f = 1/2280 = 0.000439$ c/d), but the lines previously discussed may be seen as bands at 0.962, 1.034, 1.073, 1.110 and 1.147 c/d. The width of these bands, approximately 0.008 c/d, contrasts with the width of the solar diurnal peak of 0.0013 c/d (which is the natural width of a sinusoidal signal, for the present length of data and degree of smoothing), and substantiates the view that these sidebands arise from solar rotation.

Analysis at this resolution also splits the solar diurnal and semi-diurnal peaks into lines at 1, 2 c/d and sidebands at ± 0.0027, ± 0.0055 c/d ($1/365 = 0.00274$). There is a large annual variation in the solar radiation incident on the atmosphere at Abinger, and since the amplitudes of the solar diurnal and semi-diurnal lines are affected by solar radiation both through the solar atmospheric tide and through the conductivity of the ionosphere, the annual radiation change will produce both annual and semi-annual sidebands. The ratio of power in the main peak to the annual and semi-annual sidebands is close to 1 : 0.1 : 0.01. This implies, somewhat surprisingly, that there is a large change in the solar daily variation with season, the summer amplitude being of order three times the winter amplitude. Leaton *et al.* (1963) find a ratio of 2.2 between the maximum (June) amplitude and the minimum (December) amplitude.

No 27-day sidebands of the lunar semi-diurnal line at 1.932 c/d are seen in the high resolution spectrum, but, since there is an annual change in the mean ionospheric conductivity, splitting of the line is expected. The peaks at 1.935 and 1.927, and the minor peak at 1.9295, may be merely noise fluctuations, but they are exactly where annual and semi-annual sidebands would be expected. None of these peaks on its own is significant, but together they almost certainly represent splitting of the lunar semi-diurnal magnetic variation.

8. CONCLUSIONS

The amplitude spectra obtained here (top panels of figure 3) have high stability, in the sense that the ratio of 'data points used' to 'frequency estimates obtained' was 34. The method developed here is not suitable where the data are limited and low stability spectra are required (to obtain sufficient resolution), as in the high resolution analysis in § 7. In this latter case, noise cannot be removed from the spectral estimates, and the frequency analysis will not give reliable values for the amplitudes of the lines in the spectrum.

With the use of epochs of data of length *ca.* 1 year, the method may be used to, say, determine amplitudes of magnetic variations at different parts of the sunspot cycle. One cannot select days for analysis, so that it is not possible with this method to determine amplitudes at, say, different levels of magnetic activity. It is also not possible to determine amplitudes at different seasons of

the year, or for each month of the year, since then the epochs of data would be so short (4 months or 1 month respectively) that the lunar and solar lines would not be adequately resolved.

The above are the limitations of the method of time series analysis developed here. The advantage of the method is that it provides a fast computational route to an amplitude spectrum from which numerical values may be obtained, since the estimates are free of systematic bias.

APPENDIX A. RELATION BETWEEN AUTOCORRELATION POWER ESTIMATES AND FOURIER TRANSFORM POWER ESTIMATES

Let the real data series by X_j, $j = (0, N-1)$. Take N to be even. Define the discrete direct Fourier transform Y_k by

$$Y_k = \frac{1}{N} \sum_{j=0}^{N-1} X_j W^{jk} \quad [k = (0, N-1)], \tag{A 1}$$

where $W = \exp(i2\pi/N)$.

Therefore the Fourier transform power estimates, F_k, are

$$F_k = Y_k Y_k^* = \frac{1}{N^2} \left(\sum_{j=0}^{N-1} X_j W^{jk} \right) \left(\sum_{l=0}^{N-1} X_l W^{-lk} \right)$$

$$= \frac{1}{N^2} \sum_{j=0}^{N-1} \sum_{l=0}^{N-1} X_j X_l W^{k(j-l)}. \tag{A 2}$$

For $j > l$, put $j - l = p$; for $j < l$, put $l - j = q$, giving

$$F_k = \frac{1}{N^2} \left(\sum_{p=1}^{N-1} \sum_{l=0}^{N-1-p} X_{l+p} X_l W^{kp} + \sum_{l=0}^{N-1} X_l X_l + \sum_{q=1}^{N-1} \sum_{j=0}^{N-1-q} X_j X_{j+q} W^{-kq} \right). \tag{A 3}$$

Define

$$C_m = \frac{1}{N} \sum_{l=0}^{N-1-m} X_{l+m} X_l, \tag{A 4}$$

where C_m is a biased estimate of the sample autocorrelation function (the unbiased estimate is $C_m N/(N-m)$).

Thus

$$F_k = \frac{1}{N} \left(\sum_{m=1}^{N-1} C_m (W^{km} + W^{-km}) + C_0 \right) \quad [k = (0, N-1)]. \tag{A 5}$$

Since $F_k = F_{N-k}$, there are only $\frac{1}{2}N + 1$ independent power estimates; $k = \frac{1}{2}N$ corresponds to the Nyquist frequency.

Therefore

$$F_k = \frac{1}{N} \left(C_0 + 2 \sum_{m=1}^{N-1} C_m \cos(2\pi km/N) \right) \quad [k = (0, \tfrac{1}{2}N)]. \tag{A 6}$$

The autocorrelation power estimates, at M lags, are given by (Blackman & Tukey 1958):

$$A_k^M = \frac{1}{N} \left(C_0 + 2 \sum_{m=1}^{M-1} C_m \cos(\pi km/M) \right) \quad [k = (0, M-1)]. \tag{A 7}$$

Therefore, at maximum resolution, i.e. N lags,

$$A_k^N = \frac{1}{N} \left(C_0 + 2 \sum_{m=1}^{N-1} C_m \cos(\pi km/N) \right) \quad [k = (0, N-1)], \tag{A 8}$$

and there are N independent power estimates. The Fourier transform contains phase as well as amplitude information; in calculating power from Fourier transforms, the phase information is lost, so that only half as many power estimates may be obtained from the Fourier transform as from the auto-correlation function.

Now let equation (A 1) hold for k = half-integers = $\frac{1}{2}p$, giving

$$F_{\frac{1}{2}p} = \frac{1}{N}\left(C_0 + 2\sum_{m=1}^{N-1} C_m \cos(\pi pm/N)\right) \quad [p = (0, N)]. \tag{A 9}$$

Therefore $F_{\frac{1}{2}n} = A_n^N$ for $n = (0, N-1)$ and, for n even, the autocorrelation power estimate is identical to the Fourier transform power estimate.

For $n = 2p+1$, $A_{2p+1} = F_{\frac{1}{2}(2p+1)}$. The set $F_{\frac{1}{2}(2p+1)}$ may be expressed in terms of the set Y_k:

$$F_{\frac{1}{2}(2p+1)} = |Y_{\frac{1}{2}(2p+1)}|^2,$$

$$Y_{\frac{1}{2}(2p+1)} = \sum_{j=0}^{N-1} X_j W^{\frac{1}{2}j(2p+1)} = \sum_{l=0}^{N-1} \lambda_l \sum_{j=0}^{N-1} X_j W^{jl}. \tag{A 10}$$

Equating coefficients of X_j gives

$$\exp[i\pi(2p+1)j/N] = \sum_{j=0}^{N-1} \lambda_l \exp(i2\pi jl/N). \tag{A 11}$$

Therefore
$$\lambda_l = \frac{1}{N}\sum_{j=0}^{N-1} \exp[i\pi j(2p-2l+1)/N] \quad [l = (0, N-1)]$$

$$= \frac{2}{N(1 - \exp[i2\pi(p-l+\frac{1}{2})/N])} \tag{A 12}$$

$$= i/\pi(p-l+\frac{1}{2}) \quad \text{for } |p-l| \ll N. \tag{A 13}$$

Since $F_{\frac{1}{2}(p+1)} = \left(\sum_{l=0}^{N-1} \lambda_l Y_l\right)^2$, it is apparent that (i) the major contributions to $F_{\frac{1}{2}(p+1)}$ are from the Y_l for which $|p-l| \ll N$, and (ii) the odd autocorrelation power estimates, at maximum resolution, contain the phase information.

Autocorrelation power estimates at fewer lags are weighted combinations of the A_k^N. It is easily shown that A_j^M and A_k^N are related by

$$A_j^M = \sum_{k=0}^{N-1} \gamma_k A_k^N,$$

where
$$\gamma_k = (-1)^{j+1}(k/N^2\pi)\sin(\pi kM/N)/(j^2/M^2 - k^2/N^2). \tag{A 14}$$

γ_k peaks at $j/M = k/N$ and has value M/N there.

The foregoing discussion has been simplified by omitting data and lag windows. Such windows are equivalent to replacing the Y_k and A_k by weighted sums of themselves, and would obscure the above relations without significantly changing them.

Appendix B. Phases

(a) The phase of a Fourier transform estimate

Let the data series by $G \cos (2\pi f t + \phi)$ given for $0 \leqslant t \leqslant T$ at N points $0, \Delta t, ..., (N-1)\,\Delta t$. Take N to be even. The discrete Fourier transform gives estimates at frequencies $f' = k\Delta f$, where $k = (0, \frac{1}{2}N)$ and $\Delta f = 1/T$. We wish to find the phase of an estimate at $f' = n\Delta f = f - \delta f$. The phase is given by $-\tan^{-1}(B/A)$, where B, A are the sine and cosine transforms respectively of the data series.

Before the transforms are taken, the data series is multiplied by a cosine bell window. In the following, summations are replaced by integrals; the results will subsequently be shown to be correct in the discrete case.

The cosine transform is

$$A(f') = \int_0^T \tfrac{1}{2}G \cos (2\pi f t + \phi)\,(1 - \cos (2\pi t / T))\cos (2\pi f' t)\,\mathrm{d}t$$

$$= (G/16\pi)\,[\sin (2\pi T\,\delta f + \phi) - \sin \phi]$$

$$\times \left(\frac{2}{\delta f} - \frac{1}{\delta f - \Delta f} - \frac{1}{\delta f + \Delta f} + \frac{2}{f + f'} - \frac{1}{f + f' - \Delta f} - \frac{1}{f + f' + \Delta f}\right). \quad \text{(B 1)}$$

The sine transform is

$$B(f') = \int_0^T \tfrac{1}{2}G \cos (2\pi f t + \phi)\,[1 - \cos (2\pi t / T)]\sin (2\pi f' t)\,\mathrm{d}t$$

$$= (G/16\pi)\,[\cos (2\pi T\,\delta f + \phi) - \cos \phi]$$

$$\times \left(\frac{2}{\delta f} - \frac{1}{\delta f - \Delta f} - \frac{1}{\delta f + \Delta f} - \frac{2}{f + f'} + \frac{1}{f + f' - \Delta f} + \frac{1}{f + f' + \Delta f}\right). \quad \text{(B 2)}$$

Put $\delta f = x\Delta f$, then

$$A(f') = (G/16\pi)\,[\cos (\pi x + \phi)\cos \pi x]\,(a - b), \quad \text{(B 3)}$$

and

$$B(f') = (G/16\pi)\,[-\sin (\pi x + \phi)\sin \pi x]\,(a + b), \quad \text{(B 4)}$$

where

$$a = -2T/x(x - 1)\,(x + 1),$$

$$b = -2T/(2n + x)\,(2n + x - 1)\,(2n + x + 1).$$

The phase $\theta_{f'}$ is given by

$$\theta_{f'} = -\tan^{-1}[-F(n, x)\tan (\pi x + \phi)], \quad \text{(B 5)}$$

where $F(n, x) = (a - b)/(a + b)$. For $x < 1$, $n \geqslant 1$, $F(n, x) \simeq 1$ (thus for $x = 1/\sqrt{3}$ and $n = 1$, $F = 1.05$; for $x = \frac{1}{2}$ and $n = 10$, $F = 1.00009$), so that

$$\theta_{f'} \simeq (\pi x + \phi) + p\pi, \quad \text{where } p \text{ is an integer.} \quad \text{(B 6)}$$

The signs of A, B show that p must be even.

If $x = 0$, i.e. $f = f'$, then $\theta_{f'} = \phi$, so that, if a signal has a frequency exactly k/T, the phase is correctly given at estimate k. If the signal has frequency $(k + x)/T$, $x < 1$, then at the nearest estimates k and $k + 1$ the phase will be incorrect by $x\pi$ and $(x - 1)\pi$ respectively.

The equation $\theta_{f'} = \pi x + \phi$ has been derived for the continuous case. Numerical calculations show that it also holds for the discrete case. The discrete Fourier transform of a series $\cos (2\pi 30.9j/400)$, $j = (0, 399)$ gave for the phase at estimates 30, 31 and 32 angles of $+2.8274$, -0.31414, $+2.8274$ rad respectively. For these three estimates $x = 0.9$, -0.1, -1.1, so that the calculated phase in the range $(-\pi, \pi)$ is exactly πx.
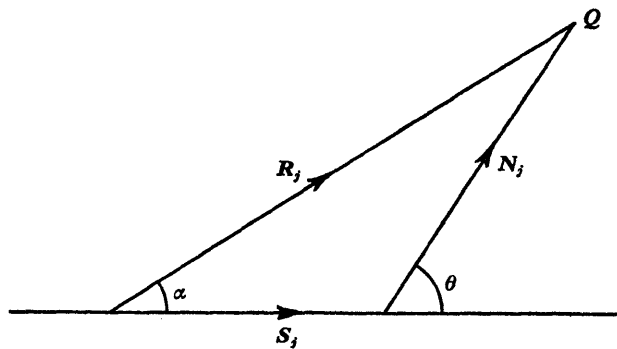
The above derivations show that unless the frequency of a signal is known exactly (i.e. x is known) then the Fourier transform estimate of phase gives no information about the phase of the signal at time $t = 0$. In the absence of noise, the estimated phase does however give the phase of the signal at time $t = \frac{1}{2}T$; $2\pi f \frac{1}{2} T = \pi(n+x)$ and, if n is even, the estimated phase is the signal phase at $t = \frac{1}{2}T$, or, if n is odd, the estimated phase differs by π from the true phase. Thus in the numerical example above, the phase at $t = \frac{1}{2}T$ is 0.9π, and this is the value obtained at estimates 30, 32.

(b) The phase between Fourier estimates from different epochs

Let the start times of two blocks of data differ by ΔT, and assume that the two blocks do not overlap (i.e. $\Delta T \geqslant T$). Then the phase of a signal of frequency $(n+x)\Delta f$, $0 \leqslant n \leqslant \frac{1}{2}N - 1$, $0 \leqslant x < 1$, will change by $2\pi(n+x)\Delta T/T$ between the start times of the two blocks. Therefore the phase of the estimates at $f' = n\Delta f$ will also change by $2\pi(n+x)\Delta T/T$ from the equation $\theta_{f'} = \pi x + \phi$ proved above. Since x is unknown, the phase change is unknown by $2\pi x \Delta T/T$, which can lie anywhere in $(-\pi, \pi)$.

APPENDIX C. ESTIMATION OF SIGNAL, NOISE AND THEIR STANDARD DEVIATIONS

(a) Distribution of R_j

S_j, N_j, R_j are the Fourier transforms at one particular frequency of the signal, noise and data respectively. Consider all the signal vectors S_j to have zero phase. Use coordinates (r, θ) with respect to the origin of the noise vectors N_j, and coordinates (R, α) with respect to the origin of the data vectors R_j. Assume $|S_j| = S$ for all j. Then the probability of the point Q lying in an area $r \, d\theta \, dr$ is assumed to be

$$P(r, \theta) \, r \, d\theta \, dr = (h^2/\pi) \, r \exp\left(-h^2 r^2\right) d\theta \, dr. \tag{C 1}$$

Therefore the probability of R_j lying in $R \, d\alpha \, dR$ is

$$P(R, \alpha) \, R \, d\alpha \, dR = (h^2/\pi) \, R \exp\left[-h^2(R^2 + S^2 - 2RS\cos\alpha)\right] d\alpha \, dR. \tag{C 2}$$

Therefore the probability of Q lying in an annulus dR is

$$P(R) \, dR = (h^2/\pi) \, R \exp\left[-h^2(R^2 + S^2)\right] dR \int_0^{2\pi} \exp\left(-2RSh^2 \cos\alpha\right) d\alpha. \tag{C 3}$$

Using Abramowitz & Stegun (1965) (subsequently referred to as A. & S.) eqn. 9.6.16 we have

$$P(R) = 2h^2 R \exp\left[-h^2(R^2 + S^2)\right] I_0(2h^2 RS), \tag{C 4}$$

where I_0 is the zero order modified Bessel function.

For calculations it is convenient to work with dimensionless numbers $R' = hR$ and $S' = hS$, so that

$$P(R')\,dR' = 2R'\exp[-(R'^2+S'^2)]\,I_0(2R'S')\,dR'. \tag{C 5}$$

The probability density function $P(R')$ is shown in figure 5 for various values of S'. For $S' = 0$, $P(R')$ is the Rayleigh distribution; as $S' \to \infty$, $I_0(2R'S') \to \exp(2R'S')/\sqrt{(4\pi R'S')}$ so that

$$P(R') \underset{S'\to\infty}{\to} 2R'\exp[-(R'-S')^2]/\sqrt{(4\pi R'S')} = \sqrt{(R'/\pi S')}\exp[-(R'-S')^2], \tag{C 6}$$

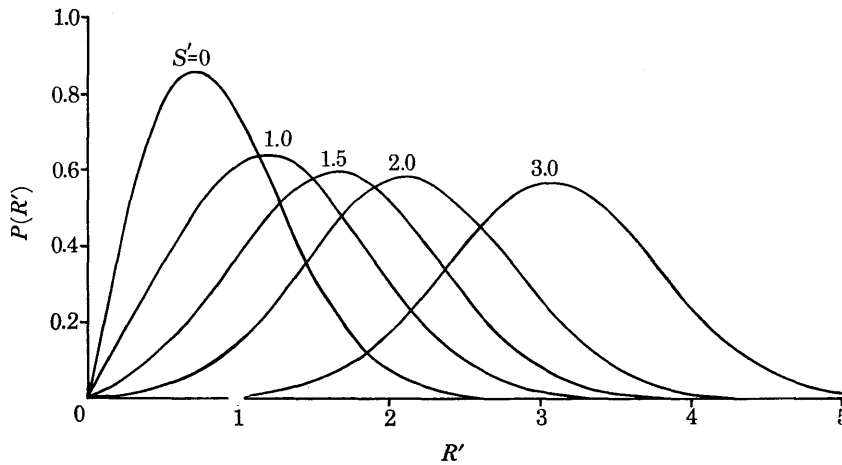i.e. for large S' (little noise) the distribution becomes a normal distribution centred on $R = S$.

FIGURE 5. Graph of $P(R') = 2R'\exp[-(R^2+S'^2)]\,I_0(2R'S')$ for various S'.

In anticipation of later results we note that the expectation of R^n, $E\{R^n\}$, is

$$E\{R^n\} = \int_0^\infty 2h^2 R^{n+1}\exp[-h^2(R^2+S^2)]\,I_0(2h^2RS)\,dR$$

$$= \exp(-h^2S^2)\,\Gamma(\tfrac{1}{2}(n+2))\,M(\tfrac{1}{2}(n+2),1,h^2S^2)/h^n \quad \text{(A. \& S., 11.4.28),} \tag{C 7}$$

where $\Gamma(x)$ is the gamma function and $M(a,b,c)$ is the confluent hypergeometric function.

Hence

$$E\{R\} = (\Gamma(\tfrac{3}{2})/h)\exp(-h^2S^2)\,M(\tfrac{3}{2},1,h^2S^2), \tag{C 8}$$

and

$$E\{R^2\} = (\Gamma(2)/h^2)\exp(-h^2S^2)\,M(2,1,h^2S^2)$$

$$= (\exp(-h^2S^2)/h^2)(1+h^2S^2)\exp(h^2S^2)$$

$$= S^2 + 1/h^2. \tag{C 9}$$

This result for $E\{R^2\}$ shows that for this model the power estimates R_j^2 are positively biased, and that the expectation of the total power is simply the sum of the signal power and the expectation of the noise power.

A further result needed later is

$$E\{RI_1(2h^2RS)/I_0(2h^2RS)\} = 2h^2\exp(-h^2S^2)\int_0^\infty R^2 I_1(2h^2RS)\,dR$$

$$= S \quad \text{(A. \& S., 11.4.28).} \tag{C 10}$$

(b) Maximum likelihood equations

We follow Kendall & Stuart (1967) here.

$P(R)$ is a function of two parameters, S and h. Let $P(R_j; S, h)$ be the value of $P(R)$ evaluated at $R = R_j$. Consider a sample of p points and define the likelihood function L by

$$L(R_1, R_2, ..., R_p; S, h) = P(R_1; S, h) P(R_2; S, h) ... P(R_p; S, h)$$

$$= (2h^2)^p \exp(-ph^2S^2) \exp[-h^2(\Sigma R_i^2)] \prod_{j=1}^{p} [R_j I_0(2h^2 R_j S)]. \qquad (C 11)$$

Maximize $\ln L$ with respect to S and h to obtain the maximum likelihood equations for $\hat{S}$ and $\hat{h}$ (estimates of S, h):

$$\frac{\partial \ln L}{\partial S} = -2ph^2S + \sum_j 2h^2 R_j I_1(2h^2 R_j S)/I_0(2h^2 R_j S), \qquad (C 12)$$

$$\frac{\partial \ln L}{\partial h} = 2p/h - 2phS^2 - 2h\sum_j R_j^2 + \sum_j 4hR_j SI_1(2h^2 R_j S)/I_0(2h^2 R_j S). \qquad (C 13)$$

Setting
$$\frac{\partial \ln L}{\partial S} = \frac{\partial \ln L}{\partial h} = 0$$

gives
$$\sum_j R_j^2/p = \hat{S}^2 + 1/\hat{h}^2, \qquad (C 14)$$

$$\sum_j R_j I_1(2\hat{h}^2 R_j \hat{S})/I_0(2\hat{h}^2 R_j \hat{S}) = p\hat{S}. \qquad (C 15)$$

Since $E\{R^2\} = S^2 + 1/h^2$, $E\{RI_1/I_0\} = S$, equations (C 14) and (C 15) give unbiased estimates of S and h.

These equations may be solved in principle by finding the minimum of

$$[\Sigma R_j^2 - p(\hat{S}^2 + 1/\hat{h}^2)]^2 + [p\hat{S} - \Sigma R_j I_1/I_0]^2;$$

this function is zero when equations (C 14) and (C 15) are satisfied, and positive everywhere else (except at $\hat{S} = 0$).

When this method of solving (C 14) and (C 15) was applied in the Abinger analysis, it was found that the available function minimization programs had trouble with the shape of the function, and took an excessive number of iterations to get sufficiently close to the zero. Alternative estimates of S and h had to be used, and a method was found that gave the same values (to the accuracy required) as equations (C 14) and (C 15).

(c) Alternative estimates of signal and noise

We have
$$\mathrm{var}(R) = E\{R^2\} - (E\{R\})^2$$

$$= S^2 + 1/h^2 - (\Gamma(\tfrac{3}{2}) M(-\tfrac{1}{2}, 1, -h^2S^2)/h)^2.$$

Let $\bar{R} = E\{R\}$, then
$$\frac{\mathrm{var}^{\frac{1}{2}}(R)}{\bar{R}} = \frac{(S'^2 + 1 - (\Gamma(\tfrac{3}{2}) M(-\tfrac{1}{2}, 1, -S'^2))^2)^{\frac{1}{2}}}{\Gamma(\tfrac{3}{2}) M(-\tfrac{1}{2}, 1, -S'^2)}$$

$$= \text{function of } S' \text{ only} \qquad (C 16)$$

Also
$$S/\bar{R} = S'/\Gamma(\tfrac{3}{2})M(-\tfrac{1}{2}, 1, -S'^2). \qquad (C 17)$$

Figure 6 shows $\mathrm{var}^{\frac{1}{2}}(R)/\bar{R}$ and $S/\bar{R}$, both as functions of S'. From the p values of R_j, $\mathrm{var}^{\frac{1}{2}}(R_j)/\bar{R}_j$ gives $\hat{S}'$; this value of $\hat{S}'$ and $\bar{R}_j$ give $\hat{S}$, and hence $\hat{h}$ also.

The maximum likelihood estimates of S and h are the desired estimates. Numerical trials showed that the estimates of S and h obtained from equations (C 16) and (C 17) were the same as the estimates of S and h obtained from the maximum likelihood equations ((C 14) and (C 15)). Having established that the estimates from equations (C 16) and (C 17) were also maximum likelihood estimates, this alternative route was used in the Abinger analysis.
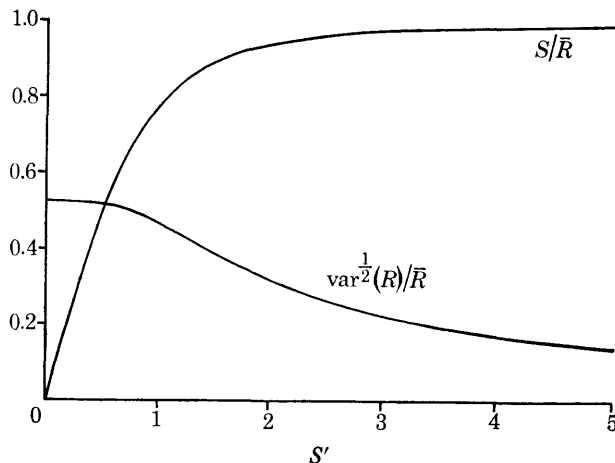

FIGURE 6. Curves of $\mathrm{var}^{\frac{1}{2}}(R)/\bar{R}$ and $S/\bar{R}$ each as a function of S'.

(d) Distribution of the maximum likelihood estimates of S and h

The method follows Kendall & Stuart (1967). As the sample size $p \to \infty$ the estimates tend to be distributed in bivariate normal form. The variances of the estimates $\hat{S}$ and $\hat{h}$, and their covariance, may be found in terms of the true values S, h of $\hat{S}$ and $\hat{h}$.

Let $\hat{\phi}_1$ = estimate of S, $\hat{\phi}_2$ = estimate of h, then

$$p\,\mathrm{cov}\,(\hat{\phi}_i, \hat{\phi}_j) = \Delta_{ij}/\Delta \quad (i,j = 1, 2),$$ (C 18)

where Δ is the determinant:

$$\Delta = \left| \int_{-\infty}^{\infty} \left(\frac{\partial \ln P(R)}{\partial \phi_i} \right)_{\phi_i} \left(\frac{\partial \ln P(R)}{\partial \phi_j} \right)_{\phi_j} P(R)\,\mathrm{d}R \right|,$$ (C 19)

and Δ_{ij} is the minor of the ith row and jth column.

Thus

$$\Delta_{22} = \int_0^\infty \left(\frac{\partial \ln P}{\partial S} \right)_S^2 P(R)\,\mathrm{d}R$$

$$= 4h^4(-S^2 + E\{R^2 I_1^2(2h^2 RS)/I_0^2(2h^2 RS)\}).$$

No analytical evaluation of $E\{R^2 I_1^2/I_0^2\}$ has been obtained, but numerical integrations show that

$$E\{R'^2 I_1^2(2R'S')/I_0^2(2R'S')\} = S'^2 + x(S'),$$ (C 20)

where $0 \leqslant x < \frac{1}{2}$ for $0 \leqslant S' < \infty$. x is plotted as a function of S' in figure 7.

Therefore

$$\Delta_{22} = 4xh^2.$$ (C 21)

Similarly

$$\Delta_{11} = 4(1 - 2h^2 S^2(1 - 2x))/h^2,$$ (C 22)

and

$$\Delta_{21} = \Delta_{12} = -4hS(1 - 2x).$$ (C 23)

From (C 18), $\text{var}\,(\hat{S}) = (1 - 2h^2S^2(1 - 2x))/4ph^2(x - h^2S^2(1 - 2x))$,   (C 24)

$$\text{var}\,(\hat{h}) = h^2x/4p(x - h^2S^2(1 - 2x)),$$ (C 25)

and correlation of $\hat{S}$ and $\hat{h} = \text{cor}\,(\hat{S}, \hat{h}) = \text{cov}\,(\hat{S}, \hat{h})/\text{var}^{\frac{1}{2}}\,(\hat{S})\,\text{var}^{\frac{1}{2}}\,(\hat{h})$

$$= h^2S^2(1 - 2x)/x(1 - 2h^2S^2(1 - 2x))^{\frac{1}{2}}.$$ (C 26)

S and h are unknown, but approximate values of var $(\hat{S})$, var $(\hat{h})$, and cor $(\hat{S}, \hat{h})$ may be obtained by substituting $\hat{S}$ for S, $\hat{h}$ for h, and using $\hat{h}\hat{S}$ to find x from figure 7.
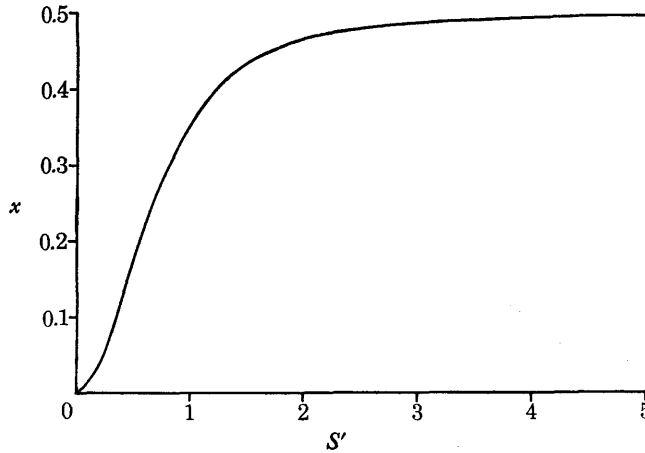

FIGURE 7. $x = E\{R'^2I_1^2/I_0^2\} - S'^2$, as a function of S'.

(e) Test of goodness of fit between $P(R)$ and the sample distribution of R_j

We wish to test the hypothesis that the sample $R_j, j = (1, p)$, is a sample from the distribution $P(R)$ derived in appendix C (a). Seventeen R_j were calculated at each frequency in the analysis of Abinger data, but this is too small a sample to use a χ^2 goodness of fit test.

Instead the Kolmogorov–Smirnov test may be used. The true values h, S of the parameters of the parent distribution $P(R)$ are unknown, but estimates $\hat{h}$, $\hat{S}$ may be obtained from the R_j. The Kolmogorov–Smirnov test assumes that the parent distribution is known exactly; the estimation of parameters of the parent distribution from the sample gives, in some sense, the best fit between the parent and sample distributions. Thus a good fit is to be expected, but, if the test shows the fit is bad, then the hypothesis that the sample R_j has a distribution of the form $P(R)$ (for any h, S) must be rejected.

Define $G(x)$ as the cumulative distribution function

$$G(x) = \int_0^x P(R')\,\mathrm{d}R'$$

and define $G_p(x)$ as the empirical cumulative distribution function

$$= 0 \quad (x < R_1'),$$
$$G_p(x) = j/p \quad (R_j' \leqslant x < R_{j+1}'),$$
$$= 1 \quad (R_p' \geqslant x).$$

Kolmogorov's statistic is $D_p = $ least upper bound $|G(x) - G_p(x)|$, and the distribution of D_p is independent of the distribution of $G(x)$. Birnbaum (1952) has tabulated Prob $(D_p < k/p)$, $k = (1, p)$.

In figure 8 are plotted $G(x)$ and $G_p(x)$ for frequency 0.0205 c/d, at which the signal is significant at the 99 % level. At this frequency, the estimates of S, σ_S are 0.080, 0.016 min, and of h, σ_h are 14.9 and 3.7 min⁻¹. $\hat{h}\hat{S} = 1.20$, so that $G(x)$ is the curve

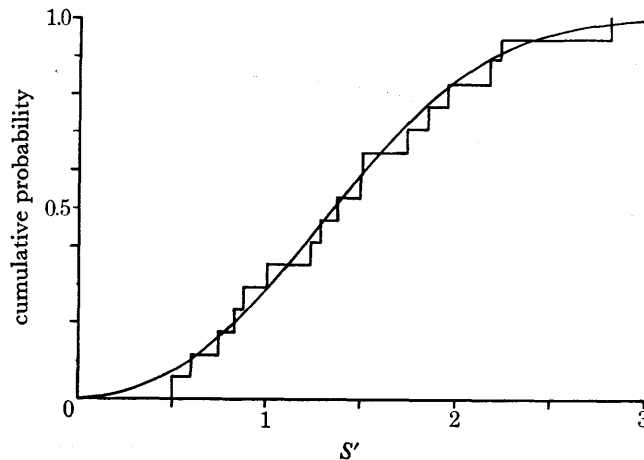$$\int_0^x P(R')\,dR \quad \text{evaluated for} \quad \hat{S}' = 1.2.$$

FIGURE 8. Kolmogorov–Smirnov test for the R_j at 0.0205 c/d, at which frequency the estimated value of S' is 1.2. The curve is

$$G(x) = \int_0^x P(R')\,dR'$$

with $S' = 1.2$; the step function is $G_p(x) = 0$ for $x < R'_1$; $= j/p$ for $R'_j \leqslant x < R'_{j+1}$; $= 1$ for $R'_p \geqslant x$. The greatest value of $|G_p(x) - G(x)|$ is 0.074.

From figure 8, $D_{17} = 0.074$, and from Birnbaum Prob $(D_{17} < 0.074) = 0.003$. The fit is therefore exceptionally good.

For frequency 0.0322 c/d, at which there is no significant signal, the test gives a probability of 0.61 for D_{17} to be less than the observed value, i.e. the fit is neither very good nor very bad.

The Kolmogorov–Smirnov test therefore gives no grounds for changing the assumptions that the signal is constant from epoch to epoch and that the noise has a Rayleigh distribution.

REFERENCES

Abramowitz, M. & Stegun, I. A. 1965 *Handbook of mathematical functions*. New York: Dover Publications.

Banks, R. J. 1968 Electromagnetic induction in the Earth. Ph.D. Thesis, University of Cambridge, England.

Bartels, J. & Johnston, H. F. 1940 Geomagnetic tides in horizontal intensity at Huancayo. *Terr. Magn. atmos. Elect.* **45**, Pt. I, 269–308, pt. II, 485–512.

Birnbaum, Z. W. 1952 Numerical tabulation of the distribution of Kolmogorov's statistic for finite sample size. *Am. Stat. Ass.* **47**, 425.

Blackman, R. B. & Tukey, J. W. 1958 *The measurement of power spectra*. New York: Dover Publications.

Bullard, E. C., Oglebay, F. E., Munk, W. H. & Miller, G. R. 1966 *BOMM, a system of programs for the analysis of time series*. I.G.P.P., University of California, La Jolla, U.S.A.

Butler, S. T. & Small, K. A. 1963 Excitation of atmospheric oscillations. *Proc. Roy. Soc. Lond.* A **274**, 91.

Cain, J. C. 1957 An analysis of the solar and luni-solar daily variations in the geomagnetic field at Sitka, Alaska, 1902–1952. *Rep. Geophys. Inst., Univ. Alaska*, AFCRC TR 57-572.

Chapman, S. 1913 On the diurnal variations of the Earth's magnetism produced by the Sun and the Moon. *Phil. Trans. Roy. Soc. Lond.* A **213**, 279.

Chapman, S. 1957 The lunar and solar daily variations of the horizontal geomagnetic vector at Greenwich, 1848–1913, with an appendix on the lunar daily variation of magnetic declination at Pavlosk and Sitka. *Abh. Akad. Wiss. Gottingen*, no. 3.

Chapman, S. & Bartels, J. 1940 *Geomagnetism*. Oxford University Press.

Chapman, S. & Miller, J. C. P. 1940 Statistical determination of lunar daily variations in geophysical data. *Mon. Not. R. astr. Soc. geophys. Suppl.* **4**, 649.

Cooley, J. W., Lewis, P. A. W. & Welch, P. D. 1967 Historical notes on the fast Fourier transform. *Proc. I.E.E.E.* **55**, 1675.

Cooley, J. W. & Tukey, J. W. 1965 An algorithm for the machine computation of complex Fourier series. *Maths Comput.* **19**, 297.

Doodson, A. T. 1922 Harmonic development of the tidal potential. *Proc. Roy. Soc. Lond.* A **100**, 305.

Foster, M. R. & Guinzy, N. J. 1967 The coefficient of coherence: its estimation and use in geophysical data processing. *Geophysics* **32**, 602.

Goodman, N. R. 1957 On the joint estimation of the spectra, cospectrum and quadrature spectrum of a two-dimensional stationary Gaussian process. *Sci. Pap. Engng Statistics Lab., New York Univ.* no. 10.

Gupta, J. C. 1966 Lunar geomagnetic variations. *Nature, Lond.* **212**, 5062.

Gupta, J. C. & Chapman, S. 1969 Lunar daily harmonic geomagnetic variation as indicated by spectral analysis. *J. atmos. terr. Phys.* **31**, 233.

Haurwitz, B. & Chapman, S. 1967 Lunar air tide. *Nature, Lond.* **213**, 9.

Hinich, H. J. & Clay, C. S. 1968 The application of the discrete Fourier transform in the estimation of power spectra. *Rev. Geophys.* **6**, 347.

Jenkins, G. M. 1965 Some examples of and comments on spectral analysis. *Appl. Statist.* **14**, 205.

Jenkins, G. M. & Watts, D. G. 1968 *Spectral analysis and its applications*. San Francisco: Holden-Day.

Kendall, M. G. & Stuart, A. 1967 *The advanced theory of statistics*, vol. 2. London: Griffin.

Leaton, B. R., Malin, S. & Finch, H. F. 1963 Solar and lunar daily variation of the geomagnetic field at Greenwich, 1916–1957. *Roy. Obs. Bull.* no. 63.

Lindzen, R. S. 1967 Lunar diurnal atmospheric tide. *Nature, Lond.* **215**, 1260.

Matsushita, S. 1967 *Solar quiet and lunar daily variation fields. Physics of geomagnetic phenomena* (eds. S. Matsushita and W. H. Campbell), vol. 1. New York: Academic Press.

Munk, W. H. & Cartwright, D. E. 1966 Tidal spectroscopy and prediction. *Phil. Trans. Roy. Soc. Lond.* A **259**, 533.

Runge, C. 1903 *Z. Math. Phys.* **48**, 443.

Schneider, O. 1963 A generalization of the phase law of lunar geomagnetic tides. *Nature, Lond.* **199**, 548.

Shapiro, R. & Ward, F. 1966 Three peaks near 27 days in the power spectrum of the international magnetic character figure C_i. *J. geophys. Res.* **71**, 2385.

Siebert, M. 1961 Atmospheric tides. *Adv. Geophys.* **7**, 105.

Topping, J. 1960 *Errors of observation and their treatment. Inst. Phys. Monogr. (Institute of Physics Monographs for Students)*. London: Chapman & Hall.

Tschu, K. K. 1949 On the practical determination of lunar and luni-solar daily variations in certain geophysical data. *Aust. J. Sci. Res.* A **2**, 1.

Wilkes, M. V. 1962 The solar and luni-solar harmonic components of geomagnetic variation at San Fernando. *J. atmos. Terrest. Phys.* **24**, 73.